

1 **A set of methods to evaluate the below-cloud evaporation effect on local**  
2 **precipitation isotopic composition: a case study infor Xi'an, China**

3 Meng Xing<sup>1,2\*</sup>, Weiguo Liu<sup>1,2,3\*</sup>, Jing Hu<sup>1,2</sup>, Zheng Wang<sup>1,2</sup>

4  
5  
6 1. State Key Laboratory of Loess and Quaternary Geology, Institute of Earth  
7 Environment, Chinese Academy of Sciences, Xi'an, 710061, China

8 2. CAS Center for Excellence in Quaternary Science and Global Change, Xi'an,  
9 710061, China.

10 3. University of Chinese Academy of Sciences, Beijing, 100049, China

11  
12 Corresponding authors:

13 Meng Xing email address: [xingmeng@ieecas.cn](mailto:xingmeng@ieecas.cn)

14 Weiguo Liu email address: [liuwg@loess.llqg.ac.cn](mailto:liuwg@loess.llqg.ac.cn)

32 Abstract:

33 When ~~the~~ hydrometeors falls from ~~the an~~ in-cloud saturated environment towards the  
34 ground, especially in ~~the~~ arid and semi-arid regions, ~~the~~ below-cloud processes ~~could~~  
35 may heavily alter the ~~precipitation~~ isotopic composition of precipitation through  
36 equilibrium and non-equilibrium fractionations. ~~If these below-cloud processes are not~~  
37 correctly identified, and accounts for they can lead to the misinterpretation of the  
38 precipitation isotopic signal ~~if these processes cannot be properly identified~~. To  
39 correctly understand the environmental information ~~contained~~ recorded in the  
40 precipitation isotopes, qualitatively analyzing the below-cloud processes and  
41 quantitatively calculating the below-cloud evaporation effect are ~~becoming very two~~  
42 important steps. Here, based on ~~a two~~ two-years of synchronous observations of  
43 precipitation and water vapor isotopes in Xi'an, we compiled a set of effective methods  
44 to systematically evaluate the below-cloud evaporation effect on local precipitation  
45 isotopic composition. The  $\Delta d\Delta\delta$ -diagram is a tool to effectively diagnose below-cloud  
46 processes, such as equilibration or evaporation, because the isotopic differences ( $\delta^2\text{H}$ ,  
47 d-excess) between the precipitation-equilibrated vapor and the observed vapor show  
48 different pathways, shows the isotopic differences ( $\delta^2\text{H}$ , d-excess) of the precipitation-  
49 equilibrated vapor relative to the observed vapor, in which the equilibration and  
50 evaporation could lead to different pathways in the two-dimensional phase space. By  
51 using the  $\Delta d\Delta\delta$ -diagram, our data show that evaporation is the major below-cloud  
52 process in Xi'an, while snowfall samples retain the initial cloud signal because ~~of they~~  
53 are less impacted by the isotopic exchange between vapor and solid phases. Then,  
54 we chose two methods ~~To to~~ quantitatively characterize the influence of below-cloud  
55 evaporation on local precipitation isotopic composition; ~~here, we chose two methods:~~  
56 one is based on the raindrop's mass change during its falling (hereafter referred to as  
57 method 1); ~~another the other~~ is to directly calculate dependent on the variations in  
58 precipitation ~~isotopic isotopic composition variations~~ from the cloud base to the ground  
59 (hereafter referred to as method 2). By comparison, we found that there are no  
60 ~~statistical significant~~ differences between the two methods in evaluating the  
61 evaporation effect on  $\delta^2\text{H}_p$ , except for snowfall events. The slope of evaporation  
62 proportion ~~and to the difference in variation in~~  $\delta^2\text{H}$  ( $F_i/\Delta\delta^2\text{H}$ ) is ~~a little~~ slightly larger in  
63 method 1 (1.0 ‰/‰) than in method 2 (0.9 ‰/‰). Additionally, both methods indicate  
64 that the ~~evaporation effect raindrops are is~~ weakly evaporated in autumn; and ~~heavily~~  
65 heavy evaporated in spring. Through ~~the a~~ sensitivity test, we found that, in two  
66 methods, relative humidity is the most sensitive parameter ~~in both~~, while the ~~variations~~  
67 ~~of~~ temperature shows different effects on the two methods. Therefore, we concluded

68 that both methods are suited to investigate the below-cloud evaporation effect, while  
69 in method 2, other below-cloud processes, such as supersaturation, can still be  
70 included. ~~following our~~ By applying -methods 2, the diagnosis of below-cloud processes  
71 and the understanding of their effects on the precipitation isotopic composition will be  
72 improved.

## 77 **1 Introduction**

78 For the paleoenvironment, the isotopic signal of precipitation recorded in ice cores  
79 (Thompson et al., 2000; Yao et al., 1996), tree rings (Liu et al., 2004; Liu et al., 2017b),  
80 speleothems (Cai et al., 2010; Tan et al., 2014), and leaf wax of loess-paleosol  
81 deposits (Wang et al., 2018b) and lake sediments (Liu et al., 2017a, 2019) could be  
82 used to reconstruct the information of temperature, precipitation, and hydrological  
83 regimes in geologic history, as it had participated ~~into~~ the formation or ~~the~~-growth of  
84 these geological archives. For the modern environment, it could be used to  
85 quantitatively constrain~~t~~ the water vapor contribution from the end-members of  
86 advection (Peng et al., 2011), evaporation (Sun et al., 2020; Wang et al., 2016a),  
87 transpiration (Li et al., 2016; Zhao et al., 2019), and even anthropogenic activities  
88 (Fiorella et al., 2018; Gorski et al., 2015; Xing et al., 2020), as ~~self~~ is itself an important  
89 part of the hydrological cycle. Thus, the hydrogen and oxygen isotopes of precipitation  
90 are ~~one-some~~ of the most important tools to trace the hydrological cycle and climate  
91 change (Bowen et al., 2019; Gat, 1996). However, limited by the sampling and isotopic  
92 fractionation theories, there remains large uncertainty (i.e., the below-cloud  
93 evaporation intensity, the moisture recycling ratio, water molecules~~s~~ exchange between  
94 the droplet and ambient air, etc.) in deciphering the information contained in  
95 precipitation when~~by~~ using hydrogen and oxygen isotopes (Bowen et al., 2019; Yao et  
96 al., 2013).

97  
98 Below-cloud evaporation is ~~exactly~~-one of the processes that influences~~s~~ the falling  
99 raindrops and; ~~modify~~-modifies their final stable isotopic content; and thus needs to be  
100 properly evaluated. Over the past decades, to determine whether ~~the-a~~ hydrometeor  
101 has ~~been~~-evaporated during its falling, most studies have depended~~ed~~ on a second-order  
102 isotopic parameter (Dansgaard, 1964; Jeelani et al., 2018; Li and Garziona, 2017),  
103 deuterium excess (defined as  $d\text{-excess} = \delta^2\text{H} - 8 \times \delta^{18}\text{O}$ ). This parameter is

104 representative of the non-equilibrium fractionations, since light isotopes ( $^1\text{H}$  and  $^{16}\text{O}$ )  
105 equilibrate faster than heavy isotopes ( $^2\text{H}$  and  $^{18}\text{O}$ ) in different phases (Clark and Fritz,  
106 1997; Dansgaard, 1964). For raindrops, the lighter water molecules ( $^1\text{H}_2^{16}\text{O}$ )  
107 preferentially equilibrate or diffuse from the liquid phase to the gas phase during their  
108 falling through unsaturated ambient air. ~~The equilibrium fractionation would~~ does not  
109 substantially change ~~the~~ d-excess, while ~~at the~~ non-equilibrium diffusional process  
110 would result in a decrease ~~of in~~ d-excess in rain (Fisher, 1991; Merlivat and Jouzel,  
111 1979). Additionally, the slope of the local meteoric water line (LMWL) has also been  
112 widely used as a metric to infer the below-cloud evaporation effect according to the  
113 theory of water isotope equilibrium fractionation (Chakraborty et al., 2016; Putman et  
114 al., 2019b; Wang et al., 2018a). Generally, the LMWL's slope is approximately equal  
115 to 8.0 ~~belonging to in~~ equilibrium fractionation, and ~~that a slope is lower than~~ deviating  
116 from 8.0 ~~pointing is related to a~~ non-equilibrium fractionation, such as the re-  
117 evaporation of raindrops.

118

119 However, it is worth noting that the change ~~of in~~ air masses (Guan et al., 2013), ~~the~~  
120 condensation ~~in under~~ supersaturation conditions (Jouzel et al., 2013), or ~~the~~ moisture  
121 exchange in the cloud and sub-cloud layers (Graf et al., 2019) also cause large  
122 variations in the slopes and d-excess values (Putman et al., 2019a; Tian et al., 2018).  
123 Therefore, it is imperative to explore a novel method to more accurately identify the  
124 below-cloud ~~evaporation~~ processes. Recently, Graf et al. (2019) provided a new  
125 interpretive framework to directly separate the convoluted influences on the stable  
126 isotopic composition of vapor and precipitation according to the theoretical  
127 fractionation processes, especially the influences of equilibration and below-cloud  
128 evaporation. The axes of the new diagram consist of the differences,  $\Delta\delta^2\text{H}$  and  $\Delta d$ ,  
129 between the isotopic composition of ~~precipitation~~ equilibrated vapor from precipitation  
130 and near-surface observed vapor, namely, the  $\Delta\delta\Delta d$ -diagram. Compared with the  
131 slope of the LMWL or ~~the~~ d-excess, ~~the~~ below-cloud equilibration and evaporation have  
132 different spatial distributions in the two-dimensional phase space of the  $\Delta\delta\Delta d$ -diagram,  
133 which makes them more easily distinguishable. Although the  $\Delta\delta\Delta d$ -diagram gives us  
134 a new guideline to more accurately identify ~~the~~ below-cloud processes ~~evaporation~~,  
135 Graf's et al. (2019) work was only tested on a cold frontal rain event during a short  
136 time, and hence, more works needs to be done ~~for validating to validate~~ the general  
137 applicability of their framework.

138

139 The ~~initial signal~~ cloud-base signal of precipitation isotopes is important in hydrological

140 studies, and thus it is necessary to quantitatively evaluate the influence of below-cloud  
141 evaporation on its variations. Normally, the isotopic difference of raindrops between  
142 ground level and cloud base is determined by the below-cloud evaporation intensity.  
143 ~~Due to~~Because it is the difficulty of ~~difficult to~~ measuring accurately measure the vapor  
144 or precipitation isotopic composition at the cloud base, the model proposed by Stewart  
145 (1975) has been widely used to ~~estimate~~ evaluate the below-cloud evaporation effect  
146 for a long time. Based on ~~the~~ well-defined laboratory conditions, Stewart (1975)  
147 parameterized the change ~~of in~~ the isotopic composition of a falling water drop with the  
148 vapor and raindrop isotopic compositions at the cloud base, and the remaining fraction  
149 of raindrop mass after evaporation (hereafter referred to as method 1). Froehlich et al.  
150 (2008) adapted the Stewart model and then assessed the change in d-excess due to  
151 below-cloud evaporation ~~based on a simple frame~~ in the European Alps. Wang et al.  
152 (2016b) further refined the calculations of the parameters, which are used to determine  
153 the remaining fraction of raindrop mass in the Stewart model, to assess the variation  
154 in d-excess of raindrops in central Asia. However, these quantitative evaluations ~~for of~~  
155 ~~the~~ below-cloud evaporation are indirect, because the results are largely dependent  
156 on the parameter that is the remaining fraction of raindrop mass after evaporation.

157

158 In recent years, with ~~the~~ progress in optical laser systems, a relatively portable field-  
159 deployable laser spectroscopic instruments have emerged, which ~~makes the~~ allows  
160 online, autonomous, and high-frequency site measurements of the water vapor stable  
161 isotope composition to be achieved (Aemisegger et al., 2012; Christner et al., 2018).  
162 Therefore, the vapor or precipitation isotopic composition at the cloud base could be  
163 directly measured (Salmon et al., 2019), or ~~be~~ indirectly deduced from the ground-level  
164 vapor isotopic composition (Deshpande et al., 2010; Salamalikis et al., 2016). This  
165 enables us to directly calculate the influence of below-cloud processes on the  
166 precipitation isotopic composition (hereafter referred to as method 2). However, ~~thus~~  
167 ~~far, these have not been systematically compared~~ less work has systematically  
168 compared the two methods.

169

170 Here, we use ~~the~~ measurements of two-year near-ground water vapor isotope  
171 compositions, and 141 precipitation isotope compositions (including event-based  
172 snowfall samples) ~~that which~~ were collected in Xi'an (34.23°N, 108.88°E), Shaanxi  
173 ~~province~~ Province, located in the Chinese Loess Plateau (CLP). The objectives of this  
174 study are to: 1. qualitatively identify the below-cloud processes of falling raindrops by  
175 using the  $\Delta\delta\Delta$ -diagram ; 2. quantitatively evaluate the below-cloud evaporation effect

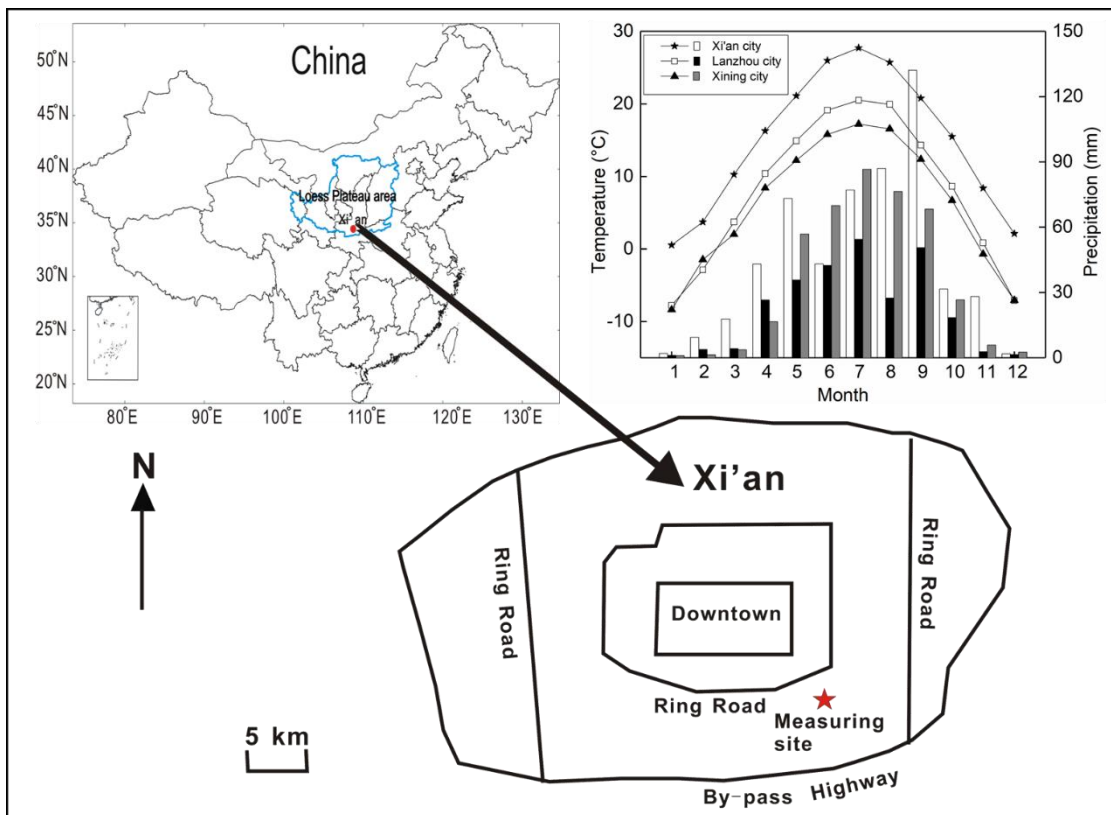
176 on precipitation isotopic composition by two methods and compare their differences;  
 177 3. understand the role of meteorological factors on ~~the~~ below-cloud evaporation and  
 178 the characteristics of below-cloud evaporation in Xi'an city. Therefore, with the  
 179 advantages of ~~the~~ paired observations of ~~the~~ vapor and precipitation isotopes near the  
 180 ground, this study will compile a set of effective methods to evaluate the below-cloud  
 181 evaporation effect on the local precipitation isotopic composition.

182

## 183 2 Data and methods

### 184 2.1 Sampling site

185 As the capital city of Shaanxi ~~province~~ Province and the largest city in ~~northwest~~  
 186 Northwest China, Xi'an is located on the Guanzhong Plain on the southern edge of the  
 187 CLP at an average elevation of 400 m. The city is located in a semi-arid to arid region  
 188 and is representative of most cities in ~~the~~ northern and northwestern of China (e.g.,  
 189 Lanzhou and Xining ~~city~~ cities, Fig. 1). The mean annual precipitation is 573.7 mm, and  
 190 the mean annual evaporation is 426.6 mm from 1951 to 2008 ~~year~~ (Wu et al., 2013).  
 191 The notable below-cloud evaporation effect has been reported in many studies for this  
 192 area (Sun et al., 2020; Wan et al., 2018; Zhu et al., 2016). Therefore, it is an ideal site  
 193 to study ~~the~~ below-cloud processes.



194 Figure 1. Average monthly variations of temperature and precipitation in Xi'an, Lanzhou, and  
 195 Xining during 2010-2015. Location of the sampling site in the Yanta Zone, 9 km SE of downtown  
 196 Xi'an. Water vapor samples are taken on the seventh floor of a twelve-story building, about

197 ~~approximately~~ 30 m above ground level. Precipitation samples are collected on the top floor, 1  
198 m above ground level.

199

200 The water vapor in ~~in~~-situ measurement site is located in a residential area,  
201 approximately 10 km southeast ~~to-of~~ downtown ~~of~~ Xi'an city (Fig. 1). The atmospheric  
202 water vapor isotopic composition was observed from 1 January 2016 to 31 December  
203 2017 on the seventh floor of the Institute of Earth and Environment, Chinese Academy  
204 of Sciences, ~~about~~~~approximately~~ 30 m above ground. The rainfall or snowfall collector  
205 was placed on the rooftop of the buildings (1 m above the floor of the roof), ~~about~~  
206 ~~approximately~~ 50 m above ground.

207

## 208 **2.2 Sampling and isotopic measurement**

209 Rainfall and snowfall samples were collected manually from the beginning of each  
210 precipitation event using a polyethylene collector (700-~~mm~~ × 450-~~mm~~ × 170 mm).  
211 Before being used, the collector was cleaned with soap and water, rinsed with  
212 deionized water, and then dried. When the precipitation event ended, the collector was  
213 quickly taken back to minimize water evaporation. The rainfall volume was measured  
214 using a graduated flask. After collection, the samples were filtered through 0.40-~~μm~~  
215 polycarbonate membranes. Then, the rainfall samples were immediately poured into  
216 100 ml polyethylene bottles. The snowfall samples were first melted at room  
217 temperature in closed plastic bags, ~~aftersecond the samples were filtration~~filtered, and  
218 then immediately poured into ~~100~~ ml polyethylene bottles. ~~About~~~~Approximately~~ a 2  
219 ml of each filtrate was transferred into a sample vial, and stored at -4 °C until ~~being~~  
220 ~~measured~~analysis. Of the ~~141~~ collected ~~144~~ samples, during the two-year sampling  
221 campaigns, 130 ~~are-were~~ rainfall samples, and the other 11 ~~are-were~~ snowfall samples  
222 (Table S3).

223

224 In all cases, the data are reported in the standard delta notation ( $\delta$ ), i.e., the per mil  
225 (‰) deviation from Vienna Standard Mean Ocean Water according to,  $\delta =$   
226  $(R_{\text{sample}}/R_{\text{reference}} - 1) \times 1000$ , where R is the isotope ratio of the heavy and light isotopes  
227 (e.g.,  $^{18}\text{O}/^{16}\text{O}$ ) in the sample and the reference.

228

229 The precipitation samples were ~~analyzed~~measured with a Picarro L2130-i (serial  
230 number HIDS 2104) wavelength-scanned cavity ring-down spectrometer ~~at-ain~~ high-  
231 precision mode. Every isotopic standard or sample was injected sequentially 8 times  
232 using a 5  $\mu\text{L}$  syringe, and then the arithmetic average of the last 3 injections was



233 accepted as the final result. All the samples were calibrated by three laboratory  
234 standards, while the  $\delta^{18}\text{O}$  and  $\delta^2\text{H}$  true values of the three laboratory standards  
235 (Laboratory Standard-1 (LS-1):  $\delta^{18}\text{O} = +0.3\text{‰}$ ,  $\delta^2\text{H} = -0.4\text{‰}$ ; Laboratory Standard-2  
236 (LS-2):  $\delta^{18}\text{O} = -8.8\text{‰}$ ,  $\delta^2\text{H} = -64.8\text{‰}$ ; Laboratory Standard-3 (LS-3):  $\delta^{18}\text{O} = -24.5\text{‰}$ ,  
237  $\delta^2\text{H} = -189.1\text{‰}$ ) are calibrated to the scale of two international standards VSMOW-  
238 GISP (Vienna Standard Mean Ocean Water -)-~~GISP~~(Greenland Ice Sheet  
239 Precipitation), with a precision of  $\pm 0.2\text{‰}$  and  $\pm 1.0\text{‰}$ , for  $\delta^{18}\text{O}$  and  $\delta^2\text{H}$ , respectively. To  
240 correct the instrument drift, the instrument was repeatedly calibrated with the  
241 laboratory standards after analyzing 8 samples. the three laboratory standards were  
242 repeatedly measured after measuring every 8 samples.  
243

244 Atmospheric water vapor  $\delta^{18}\text{O}_v$  and  $\delta^2\text{H}_v$  were also ~~measured~~analyzed by Picarro  
245 L2130-i, but ~~at-in a~~ liquid-vapor dual mode. The inlet of the gas-phase instrument is  
246 connected to the vapor source through an external solenoid valve when measuring  
247 vapor samples. This valve can switch the input of the instrument from the vapor sample  
248 to dry gas. The instrument is connected to dry gas prior to being connected to the  
249 evaporator for measuring liquid water standards so that any traces of the water vapor  
250 sample are removed from the measurement cell. The standards are injected into the  
251 evaporator with a CTC Analytics autosampler, PAL HTC-xt (Leap Technologies,  
252 Carrboro, NC, USA), and measured by the laser spectrometer. The atmospheric water  
253 vapor is pumped through a 2 m stainless-steel tube (1/8 inch) using a diaphragm pump  
254 at ~~the a~~ speed of  $4 \text{ L min}^{-1}$  and ~~also~~ detected by the laser spectrometer. The outside  
255 length of the stainless-steel tube is ~~about~~approximately 0.5 m, and the inside length  
256 is ~~approximately~~about 1.5 m. We covered the stainless-steel tube with ~~a~~ heating tape  
257 maintained at  $60 \text{ °C}$  to prevent water vapor from condensing in the stainless-steel tube.  
258 The air intake was protected with a shield to prevent rainwater from entering the  
259 sample line and direct sunlight.

260  
261 The raw water vapor  $\delta^{18}\text{O}_v$  and  $\delta^2\text{H}_v$  data were obtained at approximately ~~at~~-1 Hz and  
262 then block-averaged into 1 h intervals. As the main usage of this instrument is to  
263 measure ~~the~~ liquid water samples in our laboratory, it is used to monitor ~~the~~ water  
264 vapor isotopes in its spare time. Thus, the missing data indicate that the instrument is  
265 used for measuring liquid samples or being maintained. The event-based water vapor  
266 isotopic result is the average value from the start of the precipitation event to the end.

267  
268 The hourly meteorological data, such as temperature, relative humidity (RH), and



269 surface pressure in Xi'an, are reported by the Chinese meteorological administration,  
270 and can be downloaded from the website of <http://www.weather.com.cn/>. The  
271 meteorological station is ~~approximately~~ about 10 km to the north of our sampling site.

272

### 273 **2.3 The representativeness of ~~the~~ data**

274 ~~In~~ Over 2 years, a total of 514 days of water vapor isotopic composition measurements  
275 were carried out. For 141 precipitation samples, ~~of which~~ 100 precipitation samples  
276 have corresponding event-based water vapor isotopic results. In this study, the  
277 precipitation events mainly occurred in summer and autumn, and less frequently  
278 in winter and spring. In summer and autumn, the rainfall amount accounted for more than  
279 70% of the annual rainfall (Fig. S3). This is consistent with the multi-year average  
280 precipitation distribution in Xi'an (Fig. 1). Therefore, the collected samples are able to  
281 represent the precipitation characteristics in this region.

282

### 283 **2.4 Water vapor isotopic data correction**

284 ~~Since~~ The water vapor concentration effect and isotopic composition dependency of  
285 the cavity ringdown spectrometer have been pointed out by many studies (e.g.,  
286 Bastrikov et al., 2014; Benetti et al., 2014; Steen-Larsen et al., 2013; Weng et al.,  
287 2020), To minimize the uncertainty from the measurement, it is important to determine  
288 the isotopic composition-humidity correction response function. The humidity  
289 dependency shown in Fig. S1 also shows a dependency on the isotopic composition  
290 of the standards as reported by Weng et al. (2020). For example, in Fig. S1a and Fig.  
291 S1b, LS-1 shows a decrease in  $\Delta\delta^{18}\text{O}$  and  $\Delta\delta^2\text{H}$  with decreasing humidity, while LS-3  
292 shows an increase with decreasing humidity. Therefore, we referred to Weng ~~'s~~ et al. 's  
293 (2020) correction scheme for the isotope composition-humidity dependency.

294

295 The isotopic measurements of ground-level  $\delta^{18}\text{O}_v$  and  $\delta^2\text{H}_v$  were corrected for isotopic  
296 composition-humidity dependency using the following:

$$297 \quad \delta_{\text{meas}} - \delta_{\text{iso-hum-cor}} = \frac{a(\delta_{\text{iso-hum-cor}})}{h} + b(\delta_{\text{iso-hum-cor}}) \times h + c(\delta_{\text{iso-hum-cor}}) \quad (\text{eqEq. 1})$$

298 where  $\delta_{\text{iso-hum-cor}}$  is ~~for the~~ isotopic composition-humidity dependency corrected water  
299 vapor isotopic composition at 20000 ppmv;  $\delta_{\text{meas}}$  is the raw, measured isotopic  
300 composition at that humidity; h is the measured humidity; and a, b, and c are fitting  
301 coefficients for each water standard and isotope species. The detailed correction  
302 processes are provided in the supplementary material (Appendix A).

303

304 To calibrate the ~~measured~~-water vapor isotopic composition to the VSMOW-GISP  
 305 scale, three known-value laboratory standards ~~have been~~were used in the conversion,  
 306 while these standards were ~~measured~~analyzed in 24 h intervals to correct for  
 307 instrument drifts. The 1 $\sigma$  estimated total uncertainties are from 2.1 to 12.4 ‰ for  $\delta^2\text{H}_v$ ,  
 308 0.4 to 1.7 ‰ for  $\delta^{18}\text{O}_v$ , and 3.8 to 18.4 ‰ for d-excess<sub>v</sub> over the range of humidity from  
 309 30000 to 3000 ppmv on a 10-minute~~s~~ average through the approach using a Monte  
 310 Carlo method.

311

## 312 **2.5 Analytical methods**

### 313 **2.5.1 $\Delta d\Delta\delta$ -diagram**

314 When ~~the~~-raindrop falls from ~~the~~-cloud base to ~~the~~-ground, it continuously exchanges  
 315 with ~~the~~-surrounding vapor and may ~~lead to~~encounter net loss due to evaporation.  
 316 However, this process is ~~very hard to be~~difficult to quantified by observation. Making  
 317 use of stable water isotopes, Graf et al. (2019) introduced ~~a~~the  $\Delta d\Delta\delta$ -diagram to  
 318 diagnose the below-cloud processes and their effects on vapor and precipitation  
 319 isotopic composition, since equilibration and evaporation are two different processes  
 320 and lead to different directions in the two-dimensional phase space of the  $\Delta d\Delta\delta$ -  
 321 diagram. Here, the differences in the isotopic composition of precipitation-equilibrated  
 322 vapor relative to the observed ground-level vapor can be expressed as:

$$323 \quad \Delta\delta_v = \delta_{pv-eq} - \delta_{gr-v} \quad (\text{eqEq. 2})$$

$$324 \quad \Delta d\text{-excess}_v = d\text{-excess}_{pv-eq} - d\text{-excess}_{gr-v} \quad (\text{eqEq. 3})$$

325 where  $\delta_{pv-eq}$  and  $\delta_{gr-v}$  are the  $\delta^2\text{H}$  ( $\delta^{18}\text{O}$ ) of equilibrium vapor from precipitation and  
 326 observed vapor near the ground, respectively, and  $d\text{-excess}_{pv-eq}$  and  $d\text{-excess}_{gr-v}$  are  
 327 d-excess values of ~~the~~ equilibrium vapor from precipitation and observed vapor near  
 328 the ground, respectively. For the detailed calculation processes, please refer to the  
 329 supplemental material (Appendix B); or Graf et al. (2019).

330

### 331 **2.5.2 Below-cloud evaporation calculation: Method 1**

332 As reported by Stewart (1975), the isotopic ratio of a falling water drop is:

$$333 \quad {}^iR_{gr} = {}^i\gamma {}^iR_{va} + ({}^iR_{cb} - {}^i\gamma {}^iR_{va})F_r{}^{i\beta} \quad (\text{eqEq. 4})$$

334 where  ${}^iR_{gr}$  is the isotopic ratio of falling raindrops near the ground;  ${}^iR_{va}$  and  ${}^iR_{cb}$  are the  
 335 initial isotopic ratios for the vapor and raindrop at the cloud base;  ${}^i\gamma$  and  ${}^i\beta$  are the  
 336 parameters related to ~~the~~ equilibrium fractionation factor, relative humidity, and  
 337 molecular diffusivities; and  $F_r$  is the remaining fraction of raindrop mass after  
 338 evaporation.

339

340 Assuming that the initial isotopic composition of the raindrop at the cloud base is in  
341 equilibrium with the surrounding water vapor, Froehlich et al. (2008) adapted the  
342 Stewart model and simplified the equation to evaluate the isotopic enrichment due to  
343 below-cloud evaporation by:

$$344 \quad \Delta\delta_p = (1 - \frac{\gamma}{\alpha})(F_r^\beta - 1) \quad (\text{eqEq. 5})$$

$$345 \quad F_i = (1 - F_r) \times 100\% \quad (\text{eqEq. 6})$$

346 where  $\alpha$  is the equilibrium fractionation factor for hydrogen and oxygen isotopes; the  
347 parameters of  $\gamma$  and  $\beta$  are defined by Stewart (1975);  $F_r$  is the remaining fraction of  
348 raindrop mass after evaporation;  $\Delta\delta_p$  is the raindrop isotopic variations due to below-  
349 cloud evaporation; and  $F_i$  is the evaporation proportion. For the detailed calculation  
350 processes, please refer to the supplemental material (Appendix C); or Froehlich et al.  
351 (2008), Wang et al. (2016b), and Salamalikis (2016).

352

### 353 **2.5.3 Below-cloud evaporation calculation: Method 2**

354 Because the isotopic composition of a raindrop is directly influenced by the below-  
355 cloud processes during its falling, the below-cloud effects could be directly represented  
356 by the difference between the isotopic composition of precipitation at the ground level  
357 and cloud base:

$$358 \quad \Delta\delta_p = \delta_{gr-p} - \delta_{cb-p} \quad (\text{eqEq. 7})$$

359 where  $\delta_{gr-p}$  and  $\delta_{cb-p}$  are the isotope isotopic compositions of a falling raindrop near the  
360 ground and below the cloud base, respectively;  $\delta_{gr-p}$  and  $\Delta\delta_p$  is the raindrop isotopic  
361 variation due to below-cloud evaporation. ~~The~~  $\delta_{gr-p}$  is our observed precipitation  
362 isotopic composition, and  $\delta_{cb-p}$  is able to can be calculated based on by ground-level  
363 water vapor isotopic composition according to Deshpande et al. (2010). For the  
364 detailed calculation processes, please refer to the supplemental material (Appendix D);  
365 or Araguás-Araguás et al. (2000), Deshpande et al. (2010), and Salamalikis (2016).

366

367 Here, it should be noted that both methods use an important assumption, which is that  
368 the surface water vapor is (moist) adiabatically connected to the cloud-base water  
369 vapor. In method 1, this assumption is used to calculate the cloud base height,  
370 temperature, and pressure (Appendix C, Eq. 14-16). In method 2, the isotopic  
371 composition of the cloud-base water vapor is calculated assuming a moist adiabatic  
372 ascent of the measured ground-level water vapor (Appendix C, Eq. 22). In addition, in  
373 method 2, we assume that the raindrop isotopic composition ( $\delta_{cb-p}$ ) at the cloud base  
374 is in equilibrium with the surrounding water vapor, and the observed ground-level  
375 precipitation isotopic composition ( $\delta_{gr-p}$ ) includes the processes of evaporation, growth,

376 and isotopic equilibrium with the surrounding vapor. Furthermore, the air column is  
377 assumed to have no horizontal advection into or out of it and no updraft or downdraft  
378 of the air masses during the hydrometeors' falling. That means the vertical column at  
379 the observation site is undisturbed by horizontal movement. These assumptions only  
380 hold if a single vertical column extends from the ground to the cloud-base height. When  
381 the rain events during which the single column is affected by the surrounding air, these  
382 assumptions become invalid. ~~it should be noted that in this method we assumed that~~  
383 ~~the raindrop isotopic composition ( $\delta_{cb-p}$ ) at the cloud base is in equilibrium with the~~  
384 ~~surrounding water vapor, and the observed ground-level precipitation isotopic~~  
385 ~~composition ( $\delta_{gr-p}$ ) includes the processes of evaporation, growth, and isotopically~~  
386 ~~equilibrium with the surrounding vapor. In addition, during the hydrometeors falling we~~  
387 ~~assumed that there is no horizontal advection into or out of the column, and no updraft~~  
388 ~~or downdraft.~~ The equilibrium exchange process is not separated from the  
389 evaporation, ~~;~~ therefore, the  $\Delta\delta$  results may underestimate the below-cloud  
390 evaporation effect in method 2. To ~~get obtain~~ accurate results, more works is needed  
391 to separate ~~the~~ equilibration process from the evaporation in ~~the~~ future.

392  
393 Actually, method 1 makes use of the mass change of the falling raindrop to evaluate  
394 the below-cloud evaporation effect on isotopic composition, while method 2 evaluates  
395 its effect by directly measuring the variations ~~of in~~ isotope composition.

#### 397 **2.5.4 Statistical Analysis**

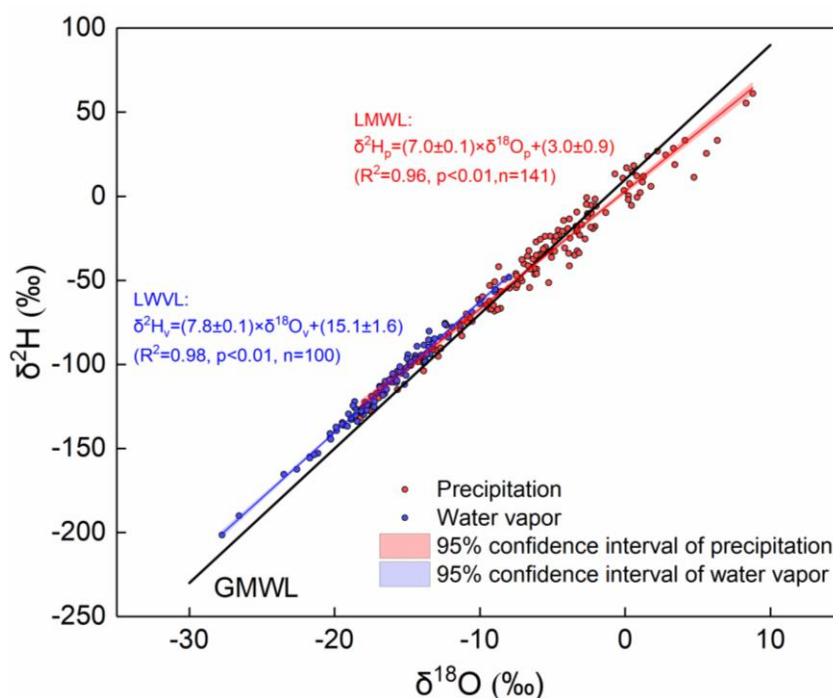
398 To compare the difference between the two methods, the independent t\_-test was  
399 performed on ~~Statistical Package for Social Sciences SPSS 13.0~~ (SPSS 13.0, Inc.,  
400 Chicago, US). ~~followed by setting the A-significant statistical difference was set at the~~  
401  ~~$p \leq 0.05$  level of confidence.~~

### 403 **3 Results and discussion**

#### 404 **3.1 Relationship between water vapor and precipitation isotopic compositions**

405 Influenced by ~~the~~ below-cloud evaporation, the slope of the local meteoric water line  
406 (LMWL) would be lower than 8, the precipitation isotopic composition would become  
407 more positive, the d-excess of precipitation would be less than 10, and the equilibrated  
408 water vapor isotopic composition would be more positive than the observed one. As  
409 shown in Fig. 2, the LMWL is defined as:  $\delta^2H_p = 7.0 \times \delta^{18}O_p + 3.0$  based on the event  
410 precipitation isotopic composition, and the local water vapor line (LWVL) is defined as:  
411  $\delta^2H_v = 7.8 \times \delta^{18}O_v + 15.1$  based on the per-precipitation-event water vapor isotopic

412 composition. Both the slope and intercept of the LMWL are lower than the ~~Global-global~~  
 413 ~~Meteoric-meteoric Water-water Line-line~~ (GMWL), which ~~are~~ has a slope of 8.0 and  
 414 intercept of 10.0 (Dansgaard, 1964; Gat, 1996), ~~respectively~~, indicating the potentially  
 415 significant below-cloud evaporation effect on precipitation (Froehlich et al., 2008). In  
 416 general, the slopes of the meteoric water lines are indicative of kinetic processes  
 417 superimposed on the equilibrium fractionation, and the ~~little-somewhat~~ lower slope of  
 418 the LWVL (slope=7.8) than the expected equilibrium fractionation (slope=8.0) may also  
 419 be related to the increasing influence of kinetic processes (Rangarajan et al., 2017).

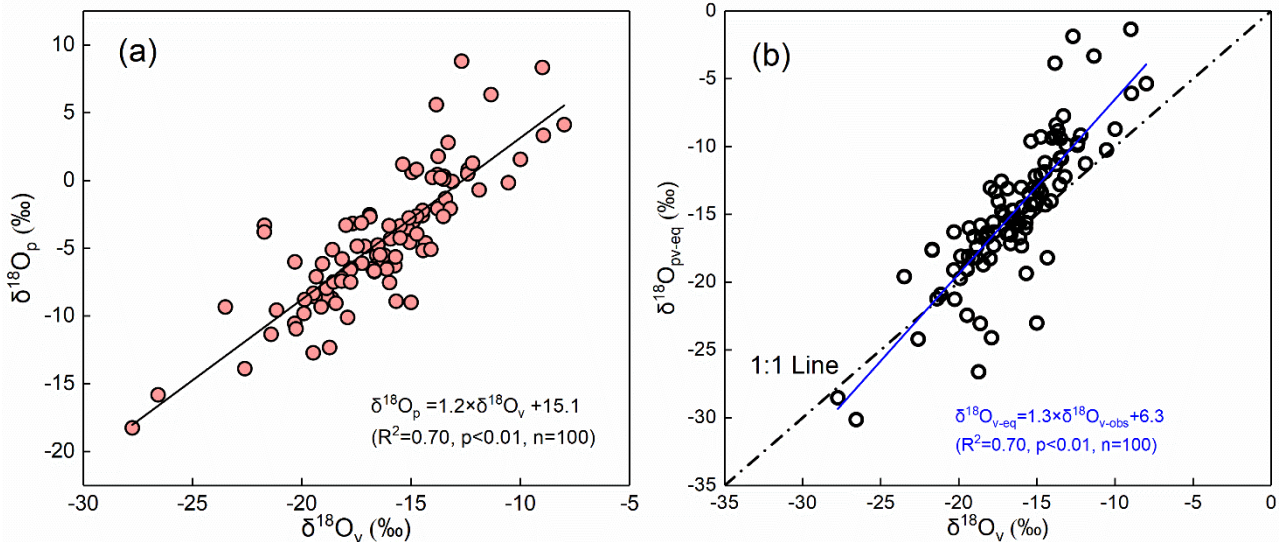


420 Figure 2. Local meteoric water line (LMWL) and ~~l~~Local water vapor line (LWVL) in Xi'an city.  
 421

422 ~~Besides~~ In addition, we noted that the water vapor and precipitation isotopic  
 423 compositions were basically distributed d in different ranges values, ~~which-with~~  
 424 the former is-being generally more negative than the latter (Fig. 2). According to the  
 425 classical isotopic fractionation theory, ~~the~~ heavier isotopes preferentially condense into  
 426 the liquid phase during the precipitation process, which results in the precipitation  
 427 isotopic composition being more positive than the water vapor ~~one-isotopic~~  
 428 composition (Dansgaard, 1964). Hence, the distribution characteristics of water vapor  
 429 and precipitation on the  $\delta^{18}\text{O}$ - $\delta^2\text{H}$  plot would make us suppose that their isotopic  
 430 compositions are in or close to equilibrium in-at this study site. To validate our  
 431 assumption, we plot their relationship in Fig. 3a. As expected, they show a significant  
 432 positive correlation ( $R^2=0.70$ ,  $p<0.01$ ), and thus, the water vapor isotopic composition  
 433 can explain 70% of the variation of-in-the precipitation isotopic composition.

434 Further~~more~~, we used the measured precipitation isotopic composition to deduce the  
 435 water vapor isotopic composition at the ground level according to the liquid-vapor  
 436 equilibrium isotope fractionation ( $\delta^{18}\text{O}_{\text{pv-eq}}$ ), and compared it with ~~the~~ observed water  
 437 vapor ( $\delta^{18}\text{O}_v$ ) in Fig. 3b. The scatterplot of the observed  $\delta^{18}\text{O}_v$  against the equilibrated  
 438  $\delta^{18}\text{O}_{\text{pv-eq}}$  also presents a significantly positive relationship (Fig. 3b).

439



440 Figure 3. Relationship between  $\delta^{18}\text{O}_p$  of precipitation and  $\delta^{18}\text{O}_v$  of water vapor in Xian (a); and  
 441 the relationship between the equilibrium computed  $\delta^{18}\text{O}_{\text{pv-eq}}$  based on the precipitation isotopic  
 442 composition and the near ground observed  $\delta^{18}\text{O}_v$  (b). The dashed-dotted line in (b) ~~stands~~  
 443 ~~represents~~ for the 1:1 line, and the blue line represents the regression line of the data.

444

445 In ~~Fig. 3b~~ the relationship plot, we also noted that the equilibrated  $\delta^{18}\text{O}_{\text{pv-eq}}$  is relatively  
 446 more positive than the observed  $\delta^{18}\text{O}_v$ . (~~Fig. 3b~~). Because Xi'an city belongs to ~~the a~~  
 447 semi-arid area, ~~the raindrops is are~~ likely to ~~be~~ evaporated in ~~the an~~ unsaturated  
 448 environment during ~~its~~ falling. Therefore, the positive  $\delta^{18}\text{O}_{\text{pv-eq}}$  is caused by the non-  
 449 equilibrium fractionation in low relative humidity, which makes the  $\delta^{18}\text{O}_{\text{pv-eq}} - \delta^{18}\text{O}_v$  points  
 450 ~~deviation deviate~~ from the 1:1 line.

451

452 The reasonable agreement of observed and equilibrated water vapor isotopic  
 453 compositions has been reported by Jacob and Sonntag (1991), Welp et al. (2008), and  
 454 Wen et al. (2010), ~~);~~ however, they postulated the different relationships underlying ~~the~~  
 455  $\delta^{18}\text{O}_v$  and  $\delta^{18}\text{O}_{\text{pv-eq}}$ . Jacob and Sonntag (1991) suggested that the water vapor isotopic  
 456 composition ~~is possible to can~~ be deduced from the corresponding precipitation isotopic  
 457 composition, but Wen et al. (2010) speculated that the equilibrium method cannot  
 458 accurately predict the ground-level water vapor isotopic composition in arid and  
 459 semiarid climates because ~~of two the~~ monthly equilibrated water vapor values ~~in April~~



460 ~~and November deviating deviate~~ from the observed values. Here, with two ~~-years~~ of  
461 continuous observations, the mean difference between ~~the~~  $\delta^{18}\text{O}_v$  and  $\delta^{18}\text{O}_{pv\text{-}eq}$  is  $-1.1\text{‰}$   
462 for  $\delta^{18}\text{O}$ ,  $-8.1\text{‰}$  for  $\delta^2\text{H}$ , and  $0.7\text{‰}$  for d-excess. Although there is a good relationship  
463 between  $\delta^{18}\text{O}_v$  and  $\delta^{18}\text{O}_{pv\text{-}eq}$  in our data, ~~the~~ below-cloud evaporation has a significant  
464 influence on the precipitation isotopic composition. Therefore, ~~it-cautious~~ should be  
465 ~~cautious-taken when derive-deriving~~ the water vapor isotopic composition from the  
466 precipitation ~~one~~ isotopic composition.

### 468 3.2 Below-cloud processes indicated by the $\Delta d\Delta\delta$ -diagram

469 Traditionally, to qualitatively assess the below-cloud evaporation of raindrops, the  
470 value of  $d\text{-excess}_p$  is a benchmark. Due to the differences in diffusivities of the  
471 individual water molecules in non-equilibrium fractionation, ~~therefore, it will cause~~  $d\text{-excess}_p$   
472 ~~to-will~~ deviate from  $0\text{‰}$ , which is a theoretical value under vapor-liquid  
473 equilibrium fractionation at temperatures ~~of around approximately~~  $20\text{ °C}$  (Gat, 1996).

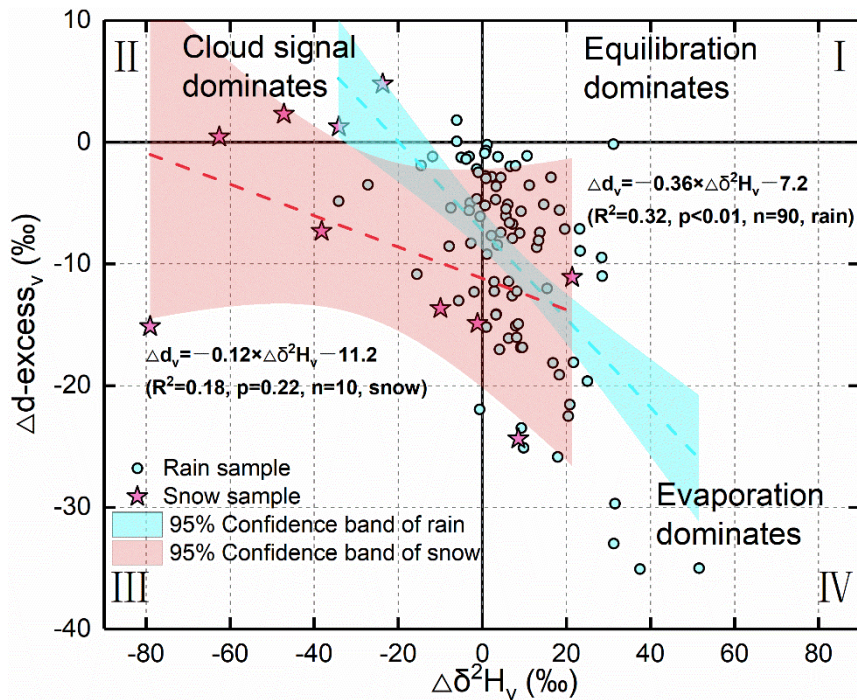
474 The global mean value of  $10\text{‰}$  for the  $d\text{-excess}_p$  in precipitation indicates that  
475 evaporation is in general a non-equilibrium process. Normally, below-cloud  
476 evaporation will decrease  $d\text{-excess}_p$ , and in comparison, mixing with the recycled  
477 water vapor from surface evaporation and plant transpiration will increase  $d\text{-excess}_p$   
478 (Craig, 1961; Dansgaard, 1964). In addition, in the water molecules diffusion process,  
479 the water vapor  $d\text{-excess}_v$  may be modified, ~~and this which~~ enhances the uncertainty  
480 ~~to-gauge in gauging~~ the below-cloud evaporation process by solely using  $d\text{-excess}_p$ . In  
481 contrast, the  $\Delta d\Delta\delta$ -diagram introduced by Graf et al. (2019) provides ~~richer~~ more  
482 information on ~~the~~ below-cloud processes.

484 Theoretically, on the  $\Delta d\Delta\delta$ -diagram,  $\Delta d < 0\text{‰}$  and  $\Delta\delta > 0\text{‰}$  indicate the below-cloud  
485 evaporation process;  $\Delta\delta < 0\text{‰}$  represents that the falling raindrop is less influenced by  
486 below-cloud evaporation and retains the cloud signals; and  $\Delta d$  and  $\Delta\delta$  close to  $0\text{‰}$   
487 suggest equilibrium conditions. By projecting our data on the  $\Delta d\Delta\delta$ -diagram, the  
488 evaporation, equilibration, and non-exchange (e.g., a snowfall event, or a transition  
489 from rain to snow with a stronger cloud signal) processes could be clearly differentiated.  
490 It is apparent ~~from in~~ Fig. 4 that most of the rainfall samples are located in the fourth  
491 quadrant with positive  $\Delta\delta^2\text{H}_v$  and negative  $\Delta d\text{-excess}_v$ , indicating that evaporation is  
492 the major below-cloud process. Interestingly, most of the snowfall samples seize the  
493 second and third quadrants with negative  $\Delta\delta^2\text{H}_v$ , which is suggestive of below-cloud  
494 evaporation with less impact on them, and their initial signals are well retained after  
495 ~~the~~ cloud-based equilibrium fractionation.



496

497 ~~According to~~Based on the results ~~of from~~ numerical simulations and in-situ  
498 observations, Graf et al. (2019) ~~summarized concluded~~ that raindrop size and  
499 precipitation intensity ~~appear to be are the two~~ important ~~driving factors of for~~  
500 ~~determining the~~ below-cloud processes, ~~because For example, precipitation with~~  
501 ~~raindrops with large raindrops diameters~~ and heavy ~~precipitation intensities will is less~~  
502 ~~affected by below-cloud processes because of the reduce their shorter~~ residence time  
503 ~~of raindrops~~ in the atmospheric column ~~with a faster fall velocity, . Therefore, and~~  
504 ~~thereby lower they are less affected by~~ the evaporation ~~and equilibration processes~~  
505 ~~possibility during on~~ their ~~falling way down~~ toward the ground surface, ~~and the  $\Delta\delta^2H_v$~~   
506 ~~is more negative. However~~It is worth noting that, ~~in the case of not considering the~~  
507 ~~factors of raindrop size and rain rate, the different precipitation types also show a clear~~  
508 ~~distribution on the  $\Delta d\Delta\delta$ -diagram, as for as almost all the snowfall event samples have,~~  
509 ~~negative  $\Delta\delta^2H_v$  values (Fig. 4)~~it seems unreasonable to explain ~~the strongly negative~~  
510  ~~$\Delta\delta^2H_v$  by the raindrop size and rain rate (Fig. 4). It is well known that Theoretically,~~  
511 snowfall events ~~normally happen occurs~~ in low-temperature conditions, ~~and~~  
512 corresponds to weak evaporation, ~~in Furthermore addition, the~~ diffusion speed of ~~the~~  
513 ~~the~~ ice phase (solid) to vapor is lower than that of liquid to vapor. Hence, ~~rain/snow~~  
514 ~~formed~~ under such ~~circumstances conditions~~, their isotopic signals ~~of rain/snow will~~  
515 ~~be are~~ less ~~impacted affected~~ by the ~~below-cloud processes environmental factors~~  
516 during ~~its~~ falling. This leads ~~the  $\Delta\delta$~~  to be more negative with ~~the decrease of decreasing~~  
517 temperature, such as the ~~observed phenomenon observed in the post-frontal~~  
518 ~~precipitation isotopes~~ in Graf's et al.'s (2019) study ~~during the post-frontal periods.~~  
519 ~~Furthermore~~Additionally, on the  $\Delta d\Delta\delta$ -diagram, the snow samples with positive  $\Delta d$ -  
520 excess<sub>v</sub> (in the second quadrant) may be related to the supersaturation process, as  
521 the liquid has unusually high  $d$ -excess<sub>p</sub> for the non-equilibrium fractionation of  
522 supersaturation (Deshpande et al., 2013; Jouzel and Merlivat, 1984). ~~Our results~~  
523 ~~suggest~~We conclude that in addition to raindrop size and rain rate, precipitation type  
524 is also an essential factor ~~that in determining influences the data distributions of the~~  
525 ~~data~~ on the  $\Delta d\Delta\delta$ -diagram.



526 Figure 4. The projection of our data on the suggested  $\Delta d\Delta\delta$ -diagram by Graf et al. (2019). The  
 527 solid lines stand for represent  $\Delta d$ -excess<sub>v</sub> and  $\Delta\delta^2H_v$  of 0‰. The dashed line corresponds to the  
 528 linear fit through the samples with the 95% confidence band in shading. The red line is for  
 529 rainfall samples, and the cyan line is for snowfall samples. The upper-Roman numerals  
 530 represent the category of the quadrant.

531

532 In Fig. 4, the slope of  $\Delta d/\Delta\delta$  is -0.36 for the rainfall samples and -0.12 for the snowfall  
 533 samples. In Graf's et al.'s (2019) study, they reported a  $\Delta d/\Delta\delta$  slope of -0.3. It should  
 534 be noted that the slope of Graf's et al. (2019) is based on intra-event samples (from  
 535 the start to the end of precipitation, each interval of 10 min to collect one sample), while  
 536 ours is based on per-event samples (only collect one sample was collected in each  
 537 precipitation event). Although the time scale is different in the two studies, interestingly,  
 538 the rainfall slopes are close to each other, while the snowfall slope is obviously different  
 539 from the rainfall slope. The  $\Delta d/\Delta\delta$  slope of -0.3 could represent a general characteristic  
 540 of rainfall for continental mid-latitude cold front passages (Graf et al., 2019). Xi'an city  
 541 is located near the 35°N in inland of China, which just belongs to the scope of  
 542 continental mid-latitude region. In comparison, the  $\Delta d/\Delta\delta$  slope of our snow samples  
 543 is less negative. Therefore, the different  $\Delta d/\Delta\delta$  slopes might be related to the different  
 544 climatic characteristics or precipitation types. Certainly, to validate this assumption,  
 545 more works needs to be done in future studies.

546

### 547 3.3 Comparing and analyzing the two methods

548 The  $\Delta d\Delta\delta$ -diagram provides rich-valuable information on the below-cloud processes,  
 549 but it is only a qualitative analysis. In comparison, the quantitative evaluation is more

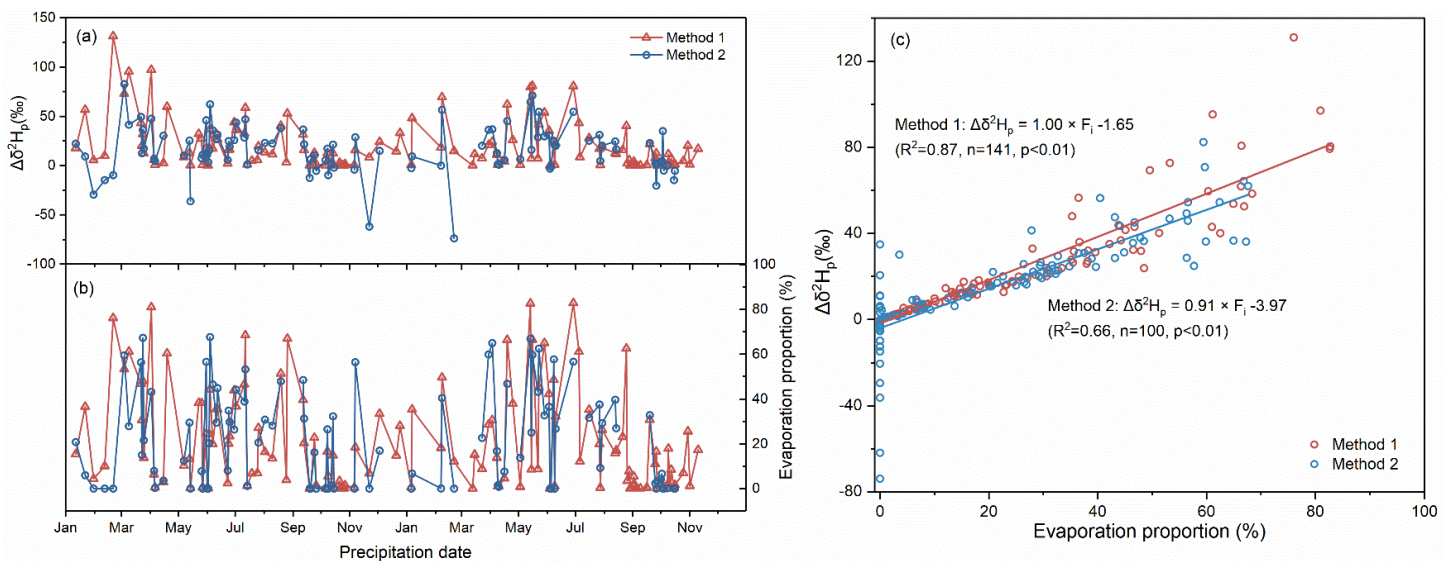
550 important to identify the below-cloud evaporation effect. Here, we chose two methods  
551 to ~~respectively~~ calculate the variations ~~of in~~  $\Delta\delta^2H_p$  and ~~the~~ evaporation fraction ( $F_i$ ) on  
552 per-event precipitation, and compared their differences.

### 554 **3.3.1 Quantitatively ~~evaluate~~ evaluation of the below-cloud evaporation effect** 555 **by derived from the two methods**

556 The  $\Delta\delta^2H_p$  ranges s from 0 to 131.1 ‰ with an average and standard deviation of  $17.8$   
557  $\pm 23.8$  ‰, and the  $F_i$  ranges s from 0 to 82.7% with an average and standard deviation  
558 of  $16.3 \pm 21.9$ % (n=141) for method 1. The  $\Delta\delta^2H_p$  ranges s from -73.8 to 82.5 ‰ with  
559 an average and standard deviation of  $16.3 \pm 24.4$  ‰, and the  $F_i$  ranges s from 0 to 67.6%  
560 with an average and standard deviation of  $22.1 \pm 21.7$ % (n=100) for method 2. For  
561 the 90 rainfall events with corresponding water vapor data, the average ~~±~~ and standard  
562 deviation ~~is-are~~  $18.4 \pm 21.7$  ‰ for  $\Delta\delta^2H_p$  ~~in-derived from~~ method 1, and the value is  
563  $18.7 \pm 20.6$  ‰ for  $\Delta\delta^2H_p$  ~~in-derived from~~ method 2. For the 10 snowfall events, the  
564 average ~~±~~ and standard deviation of  $\Delta\delta^2H_p$  ~~is-are~~  $42.6 \pm 43.7$  ‰ for method 1 and -  
565  $6.1 \pm 41.6$  ‰ for method 2. In the two methods, according to the independent t-test,  
566 there are no ~~statistical-significant~~ differences in the  $\Delta\delta^2H_p$  of rainfall samples ( $F=0$ ,  
567  $p=0.91$ ,  $n=90$ ), but the  $\Delta\delta^2H_p$  of snowfall shows s a large difference ( $F=0.196$ ,  $p<0.05$ ,  
568  $n=10$ ).

570 As shown in Fig. 5a and Fig. 5b, the  $\Delta\delta^2H_p$  and  $F_i$  in the two methods have similar  
571 fluctuation trends. ~~The~~ A positive  $\Delta\delta^2H_p$  and high  $F_i$  appear from March to July, while  
572 ~~the~~ a negative  $\Delta\delta^2H_p$  and low  $F_i$  ~~show-appear~~ from September to following February. In  
573 addition, the most positive  $\Delta\delta^2H_p$  values are captured by method 1, while the most  
574 negative values are detected by method 2. ~~In order to~~ To analyze the underlying reason,  
575 we checked the equation used to calculate  $\Delta\delta^2H_p$ . We noted that in ~~e~~ Eq. 5, the  $F_r$  is  
576 always lower than 1, and thus  $(F_r^\beta - 1)$  is negative. Similarly, ~~the~~  $\frac{Y}{\alpha}$  is smaller than 1, and  
577 thus,  $(1 - \frac{Y}{\alpha})$  is also negative. Therefore, the  $\Delta\delta^2H_p$  calculated by method 1 ~~could-not-be~~  
578 ~~a-negative-number~~ is always positive. In method 2, the most negative  $\Delta\delta^2H_p$  values are  
579 related to ~~the~~ snowfall events. During the supersaturation process, vapor deposition  
580 takes place over ice in the cloud (Jouzel and Merlivat, 1984) with non-equilibrium  
581 fractionation (the kinetic fractionation factor  $\alpha_k < 1$ ), leading to the effective isotopic  
582 fractionation factor ( $\alpha_{eff} = \alpha_{eq} \alpha_k$ ) being smaller than the equilibrium fractionation  
583 coefficient ( $\alpha_{eq}$ ), and resulting in the ground-observed  $\delta_{gr-p}$  of solid precipitation (snow)  
584 being more depleted than the calculated  $\delta_{cb-p}$  under equilibrium fractionation (in Eq.  
585 7). ~~During the supersaturation process, vapor deposition occurs over ice (Jouzel and~~

586 ~~Merlivat, 1984), which may cause the snow isotopic composition at the ground to be~~  
 587 ~~more depleted than its formation height.~~ In fact, the mass of ~~the~~ snow also increases  
 588 ~~in the under~~ supersaturation conditions, ~~;~~ however, method 1 only considers the  
 589 evaporation process. The diameter of the raindrop used to determine the terminal  
 590 velocity and evaporation intensity (Supplemental material, ~~eqEqs.~~ 10-13) does not take  
 591 into account ~~the different relationship of fall velocity to hydrometeor size for snowflakes~~  
 592 ~~and raindrops, the snowfall factor~~ which results in great uncertainty in method 1.  
 593 Therefore, method 1 is not suitable for evaluating the below-cloud effect on the  
 594 precipitation isotopic composition ~~when the for~~ snowfall or low-temperature rainfall  
 595 events.



596 Figure 5. The variation ~~of in~~  $\Delta\delta^2H_p$  for per-event precipitation in method 1 and method 2 (a); the  
 597 same as (a) but for  $F_i$  (b); the relationship between  $F_i$  and  $\Delta\delta^2H_p$  in method 1 and method 2 (c)

598

599 In addition, the influence of the below-cloud evaporation effect on ~~the~~  $\delta^2H_p$  is heavier  
 600 in method 1 than in method 2, especially at higher  $F_i$  conditions (Fig. 5c), because the  
 601 slope of  $F_i/\Delta\delta^2H$  in method 1 (1.00 ‰/‰) is ~~a little slightly~~ steeper than ~~that~~ in method  
 602 2 (0.91 ‰/‰), and the intercept in method 1 (-1.65) is more positive than ~~that~~ in  
 603 method 2 (-3.97). Thus, under the same evaporation intensity, ~~the~~  $\Delta\delta^2H_p$  is more  
 604 enriched in method 1 than in method 2.

605

606 On the seasonal scale, both methods show that the below-cloud evaporation effect is  
 607 heavier in spring and summer and weaker in autumn and winter (Fig. S4). Their  
 608 differences are the smallest in spring and the largest in winter. ~~The significant~~  
 609 ~~difference in winter might be related to the predominance of solid precipitation, which~~  
 610 ~~is not accounted for in method 1. The significant difference in winter might be related~~  
 611 ~~to the supersaturation process.~~



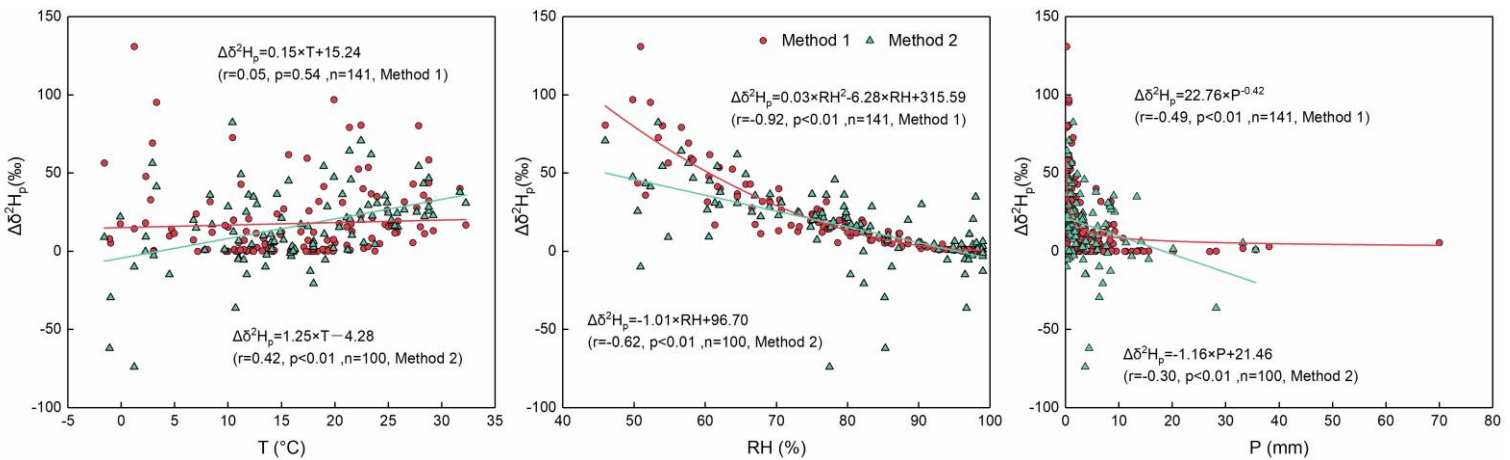
612

### 613 3.3.2 Meteorological controls on the two methods

614 To further explore the differences ~~by in employing~~ the two methods, we performed ~~the~~  
615 correlation analyses between meteorological factors and ~~the~~  $\Delta\delta^2H_p$  (Fig. 6). The results  
616 show that RH is the most important meteorological factor for both methods (Fig. 6b).

617 Furthermore, the impact of RH on the variations in  $\Delta\delta^2H_p$  is stronger in method 1 ( $r=-$   
618 0.92) than in method 2 ( $r=-0.62$ ), and this phenomenon is more obvious when the RH  
619 is lower than 60%. Although precipitation amounts have influences on both methods  
620 as well, their effect on  $\Delta\delta^2H_p$  is rather weak ( $r=-0.49$ , method 1;  $r=-0.30$ , method 2; Fig.  
621 6c), and their ~~the~~ relationships are non-linear ~~or its effect on  $\Delta\delta^2H_p$  is rather weak ( $r=-$~~   
622 0.49, method 1;  $r=-0.30$ , method 2; Fig. 6c). For temperature, in method 1, there is no  
623 clear correlation between  $\Delta\delta^2H_p$  and temperature ( $r=0.05$ ), and in method 2 their  
624 positive correlation is weak ~~in method 2~~ ( $r=0.42$ ). ~~Wang et al. (2016b) explicitly pointed~~  
625 ~~out that among the parameters of temperature, precipitation amount, RH, and raindrop~~  
626 ~~diameter, RH generally plays a decisive role on  $\Delta d$  excess in the below-cloud~~  
627 ~~evaporation process.~~

628



629 Figure 6. The correlations between ~~the~~  $\Delta\delta^2H_p$  and the temperature in method 1 (red dots) and  
630 in method 2 (green triangles) (a); the same as (a) but for RH (b); the same as (a) and (b) but  
631 for precipitation amount (c).

632

633 In both methods, in under an arid environment with high temperature, low RH, and  
634 small precipitation amounts, the evaporation effect on ~~the~~  $\Delta\delta^2H_p$  is large. However, in  
635 under the low-temperature conditions (below 5 °C), there is a divergence in  $\Delta\delta^2H_p$  for  
636 the two methods, which is partly attributed to the supersaturation condition. With ~~the~~  
637 increase of increasing RH,  $\Delta\delta^2H_p$  becomes closer to 0 in both methods, but the  
638 variation of in  $\Delta\delta^2H_p$  is large in method 2 and very limited in method 1 when the RH is  
639 higher than 80%. There is a wide range, from 0 to 130‰, for  $\Delta\delta^2H_p$  when the

640 precipitation amount is small. As the precipitation amount is above 10 mm, the value  
641 of  $\Delta\delta^2H_p$  tends toward 0-‰.

642

### 643 3.3.2 Sensitivity test

644 In method 1, the input physical parameters include temperature, RH, precipitation  
645 amount, and surface pressure. ~~In method 2, the same input parameters as for method~~  
646 ~~1 were used except for the precipitation amount. In method 2, the input parameters~~  
647 ~~include temperature, RH, and surface pressure.~~ Therefore, these parameters are  
648 considered in the sensitivity tests.

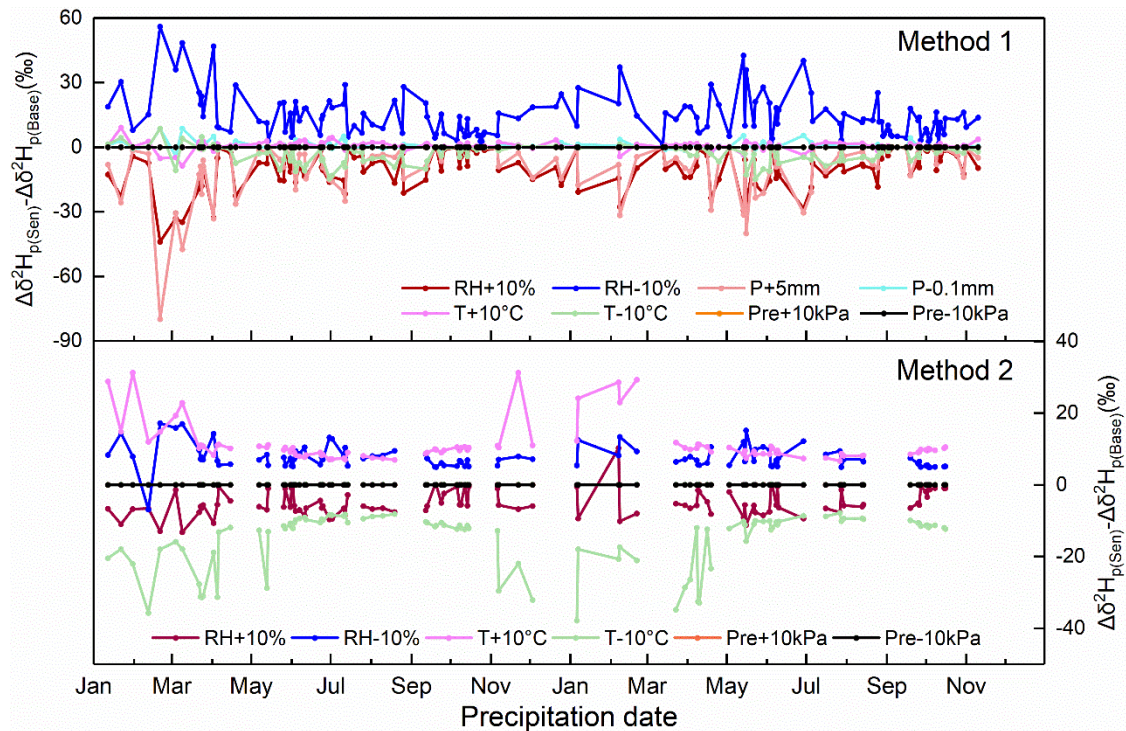
649

650 For the RH test, one case adds 10% to the measured RH, and another case subtracts  
651 10% from the measured RH. If the RH values are above 100%, then they are artificially  
652 set to 99% to conform to reality. Two temperature scenarios, plus and minus 10 °C  
653 based on the actual temperature, are analyzed. In the sensitivity test of precipitation  
654 amount, considering that the amounts are lower than 0.1 mm in some precipitation  
655 events, ~~therefore,~~ the reduction lower limit is set ~~at to~~ 0.1 mm, and the enhancement  
656 upper limit is set ~~at to~~ 5 mm. On the basic surface pressure condition, a 10 kPa  
657 pressure fluctuation is considered for its impact.

658

659 As shown in Fig. 7, the increase ~~of in~~ RH and precipitation, and decrease ~~of in~~  
660 temperature have a negative impact, ~~;~~ that is, the below-cloud evaporation effect on  
661 the isotopic composition will be attenuated. ~~On the contrary~~In contrast, the decrease  
662 ~~of in~~ RH and precipitation, and increase ~~of in~~ temperature have a positive impact,  
663 indicating that the below-cloud evaporation effect will be strengthened. The varying  
664 surface pressure has no impact on ~~the~~  $\Delta\delta^2H_p$  for both methods. Moreover, the  
665 influencing strength of the different physical parameters on ~~the~~  $\Delta\delta^2H_p$  is different in the  
666 two methods. For example, in method 1, the increase ~~of in~~ temperature basically does  
667 not change the evaporation effect on ~~the~~  $\Delta\delta^2H_p$ , and the influence of decreasing  
668 temperature on mitigating evaporation is limited as well. However, the situation is  
669 totally different in method 2, where the temperature is a decisive factor. In addition, the  
670 influence of RH is over the temperature in method 1, but the condition is reversed in  
671 method 2. The precipitation amount is also an important factor, as the influence of  
672 precipitation on  $\Delta\delta^2H_p$  even surpasses es the RH when it is increased by 5 mm. Because  
673 of the limited decrease in precipitation amount, its positive feedback is ~~hard~~ difficult  
674 to evaluate.

675



676 Figure 7. Sensitivity test of  $\Delta\delta^2H_p$  under different cases. In method 1, the cases include  $\pm 10\%$   
 677 RH,  $\pm 10^\circ\text{C}$  temperature,  $\pm 10\text{ kPa}$  surface pressure,  $+5\text{ mm}$  precipitation amount, and  $-0.1$   
 678  $\text{mm}$  precipitation amount. In method 2, the cases include  $\pm 10\%$  RH,  $\pm 10^\circ\text{C}$  temperature, and  
 679  $\pm 10\text{ kPa}$  surface pressure. The  $\Delta\delta^2H_{p(\text{Sen})}$  represents the results of the sensitivity test, and  
 680  $\Delta\delta^2H_{p(\text{Base})}$  represents the results of the base condition.  
 681

682 In the calculation process of method 2 (eqEq. 7, and supplemental material, eqEq. 22),  
 683 except for the measured ground-level precipitation and water vapor isotopic  
 684 compositions ( $\delta_{\text{gr-p}}$  and  $\delta_{\text{gr-v}}$ ), the other two controlling factors are the equilibrium  
 685 fractionation factor ( $\alpha$ ) and the cloud base height. The  $\alpha$  is determined by the  
 686 temperature variations of the cloud base, while the cloud base height is related to  
 687 surface temperature and RH (supplemental material, eqEq. 14-17). With increasing  
 688 RH increase, the cloud base heights decrease, and vice versa (Fig. S5). In comparison,  
 689 the cloud base heights are not sensitive to the changes of in temperature (Fig. S5).

690  
 691 Compared with method 2, the calculation process of method 1 is more complex. Many  
 692 variables, such as raindrop diameter, evaporation intensity, raindrop falling velocity,  
 693 and cloud base height, etc., are needed need to be considered, while they are  
 694 convoluted with temperature, RH, precipitation amount, and surface pressure. Through  
 695 the sensitivity test, RH and precipitation amount are the two decisive factors in method  
 696 1 for deciding determining the below-cloud evaporation intensity.

697

### 698 3.3.2 Uncertainty estimations



699 There are many uncertainties in the two methods' estimates. In method 1, the input  
700 parameters include the variation ~~of in~~ temperature, RH, precipitation amount, and  
701 surface pressure. In method 2, the uncertainty comes from the variations ~~of in~~ the input  
702 temperature, RH, surface pressure, ground level water vapor  $\delta^2\text{H}_{\text{gr-v}}$ , and precipitation  
703  $\delta^2\text{H}_p$ . However, the variations ~~of in~~ surface pressure show no impact on ~~the~~  $\Delta\delta^2\text{H}_p$  in  
704 the sensitivity test; therefore, ~~it is they are~~ not considered in the uncertainty calculation.

705

706 To check the influence of temperature, RH, precipitation amount, and precipitation  $\delta^2\text{H}_p$   
707 on the below-cloud evaporation effect, we assume that the errors are mainly from the  
708 measurement uncertainty of the instrument, which is  $\pm 0.3\text{ }^\circ\text{C}$ ,  $\pm 3\%$ ,  $\pm 4\%$  precipitation  
709 amount, and  $\pm 1.0\text{ ‰}$ , respectively. Due to the humidity effect (~~section Sect.~~ 2.4), the  
710 measured  $\delta^2\text{H}_{\text{gr-v}}$  for each event has a wide range of uncertainty, which varies from 1.3  
711 to 8.2‰. Hence, the lower and upper limits of the above used input parameters in for  
712 method 1 and method 2 are used to quantify the uncertainties and add them  
713 quadratically to ascertain the total uncertainty (Rangarajan et al., 2017; Wu et al.,  
714 2022). We obtain the overall uncertainty varying from 0.71 to 0.72‰ for method 1, and  
715 from 0.60 to 1.05‰ for method 2 in the estimates of  $\Delta\delta^2\text{H}_p$  values (refer to  
716 supplemental material, Appendix E).

717

### 718 **3.4 The characteristics of below-cloud evaporation effect in Xi'an**

719 ~~Since the below-cloud evaporation is very common in arid and semi-arid regions,~~  
720 ~~before exploring the information contained in the precipitation isotopes, it is important~~  
721 ~~to clearly know the variation of precipitation isotopic composition during its falling. Here,~~  
722 ~~we summarized the seasonal variations of  $\Delta\delta^2\text{H}_p$  in Xi'an by two methods (Fig. 8).~~

723 ~~Figure 8 The variations of temperature, RH, precipitation amount, and  $\Delta\delta^2\text{H}$  in four seasons in~~  
724 ~~Xi'an. In the middle of the figure, the red boxes represent the results from method 1, and the~~  
725 ~~blue boxes represent the results from method 2.~~

726

727 ~~By seasonally dividing the precipitation isotopic composition on the  $\Delta d\Delta\delta$  diagram, it~~  
728 ~~shows that samples collected in spring and summer dominate the evaporation phase,~~  
729 ~~reflecting a stronger evaporation influence, while most of the winter precipitation and~~  
730 ~~part of autumn precipitation monopolize the cloud signal phase indicating a weak or~~  
731 ~~no below-cloud evaporation, and even supersaturation on these samples (Fig. S6).~~  
732 ~~Based on quantitative analysis, the two methods show similar evaporation effect in~~  
733 ~~spring, summer, and autumn, and different trends in winter (Fig. 8). The reasons had~~  
734 ~~been discussed in Section 3.3.1. In addition, method 1 shows a narrower variation~~

735 range of  $\Delta\delta^2\text{H}_p$  than method 2, because it only considers the below-cloud evaporation  
736 process. In method 2, the evaporation effect on  $\delta^2\text{H}_p$  is powerful in spring and summer,  
737 and weaker in autumn and winter (Fig. 8). The seasonal variation of  $\Delta\delta^2\text{H}_p$  basically  
738 mirrors the trend of RH. Although the precipitation amount is highest in the summer,  
739 the temperature is extremely high and RH is relatively low, which causes the relatively  
740 positive  $\Delta\delta^2\text{H}_p$  in summer. In winter, the low  $\Delta\delta^2\text{H}_p$  in method 2 may be related to the  
741 precipitation type, because snowfall is the main deposition type in this season.

#### 743 4 Conclusions

744 The below-cloud processes of precipitation are complex, variable, and influenced by  
745 many factors, especially in arid and semi-arid regions. Previously, below-cloud  
746 evaporation ~~is~~ was the most well-studied post-condensation process with the aid of the  
747 slope of LMWL and d-excess of precipitation. In comparison, other below-cloud  
748 processes, such as ~~the~~ vapor-liquid equilibration or ~~the~~ hydrometeors supersaturation  
749 growth, have paid less attention to different rain types. In this study, based on the two-  
750 years of precipitation data collected in Xi'an, we compiled a set of methods to  
751 systematically evaluate the below-cloud evaporation effect on the local precipitation  
752 isotopic composition, and ~~get~~ obtained the following main conclusions:

753 1. In arid areas, the precipitation and water vapor isotopic compositions ~~have a good~~  
754 relationship are closely related, and ~~therefore thus~~ the joint observation of the two  
755 tracers could provide more information on ~~the~~ precipitation processes. In Xi'an, the  
756 below-cloud evaporation effect is stronger in spring and summer, and weaker in  
757 autumn and winter, and is related to the variation of in the local RH.

758 2. Our work ~~validates~~ evaluates the general applicability of the  $\Delta d/\Delta\delta$ -diagram.  
759 Although there is a difference in timescale between Graf's et al.'s (2019) study (intra-  
760 event) and ours (per-event), the influence of below-cloud processes on our  
761 precipitation and water vapor isotopic data can be clearly visualized on the  $\Delta d/\Delta\delta$ -  
762 diagram. In this study, ~~the~~ below-cloud evaporation is the main process during the  
763 raindrops falling. However, snowfall samples are less influenced by evaporation, and  
764 mainly preserve their initial water vapor information. The different  $\Delta d/\Delta\delta$  slopes of  
765 rainfall and snowfall might be related to the precipitation types.

766 3. By comparing the two methods, there are no significant differences in  $\Delta\delta^2\text{H}_p$  for  
767 rainfall events, but they show a large difference for snowfall events, and this is related  
768 to the supersaturation process not being considered in method 1 ~~we find that both~~  
769 ~~could be used to quantitatively evaluate the below-cloud evaporation effect on~~  
770 ~~precipitation except for snowfall events, because there are no statistical differences in~~

771 ~~their  $\Delta\delta^2H_p$  results~~. The slope of  $F_i/\Delta\delta^2H$  in method 1 (1.00 ‰/‰) is ~~a little slightly~~ steeper  
772 than ~~that~~ in method 2 (0.91 ‰/‰), indicating ~~the a~~ stronger evaporation effect on  $\Delta\delta^2H$   
773 for method 1. ~~However, the two methods of  $\Delta\delta^2H$  show a large difference in winter,~~  
774 ~~especially for snow samples, which is related to the supersaturation process not being~~  
775 ~~considered in method 1.~~ Through meteorology and ~~sensitivity sensitivities~~ analysis, ~~we~~  
776 ~~found that in the two methods,~~ RH is the main controlling factor, ~~and The two methods~~  
777 ~~temperature~~ shows different ~~sensitivity to impacts on the temperature~~ variations of  
778  $\Delta\delta^2H$ . Through uncertainty estimations, method 2 shows a larger uncertainty range  
779 (ranging from 0.60 to 1.05‰) than method 1 (ranging from 0.71 to 0.72‰).

780 4. Considering the assumption that the surface water vapor is (moist) adiabatically  
781 connected to the cloud-base water vapor, the validation of the two methods is for  
782 frontal precipitation or convective precipitation. Here, method 1 only includes below-  
783 cloud evaporation by construction, while in method 2, other processes can still be  
784 included, such as supersaturation. Therefore, both methods are suited to study the  
785 below-cloud evaporation effect (no significant differences in  $\Delta\delta^2H_p$  for rainfall events);  
786 however, if other below-cloud processes are included, applying method 2 is the better  
787 choice. In future studies, further high-resolution observations of vertical profiles of  
788 precipitation and water vapor isotopes, whether tower-based or aircraft-based, have  
789 the potential to greatly improve constraints on below-cloud processes.

#### 795 **Data availability**

796 The datasets can be obtained from Table S3.

#### 798 **Author contribution**

799 Meng Xing and Weiguo Liu designed the experiments, interpreted the results, and  
800 prepared the manuscript with contributions from all co-authors. Meng Xing and Jing  
801 Hu analyzed the precipitation and water vapor samples. Jing Hu maintained the  
802 experimental instruments.

#### 804 **Competing interests**

805 The authors declare that they have no conflict of interest.

806

807

## 808 **Acknowledgment**

809 This work was supported by Science Foundation of China (No. 42177093), West Light  
810 Foundation of The Chinese Academy of Sciences, and China scholarship council. The  
811 authors would like to thank Mr. Xijing Cao for helping to collect precipitation samples.

812

## 813 **References**

814 Aemisegger, F., Sturm, P., Graf, P., Sodemann, H., Pfahl, S., Knohl, A. and Wernli, H.:  
815 Measuring variations of  $\delta$  18O and  $\delta$  2H in atmospheric water vapour using two commercial  
816 laser-based spectrometers: An instrument characterisation study, *Atmos. Meas. Tech.*, 5(7),  
817 1491–1511, doi:10.5194/amt-5-1491-2012, 2012.

818 Araguás-Araguás, L., Froehlich, K. and Rozanski, K.: Deuterium and oxygen-18 isotope  
819 composition of precipitation and atmospheric moisture, *Hydrol. Process.*, 14(8), 1341–1355,  
820 doi:10.1002/1099-1085(20000615)14:8<1341::AID-HYP983>3.3.CO;2-Q, 2000.

821 Bastrikov, V., Steen-Larsen, H. C., Masson-Delmotte, V., Gribanov, K., Cattani, O., Jouzel, J.  
822 and Zakharov, V.: Continuous measurements of atmospheric water vapour isotopes in western  
823 Siberia (Kourovka), *Atmos. Meas. Tech.*, 7(6), 1763–1776, doi:10.5194/amt-7-1763-2014,  
824 2014.

825 Benetti, M., Reverdin, G., Pierre, C., Merlivat, L., Risi, C., Steen-Larsen, H. C. and Vimeux, F.:  
826 Deuterium excess in marine water vapor: Dependency on relative humidity and surface wind  
827 speed during evaporation, *J. Geophys. Res.*, 119(2), 584–593, doi:10.1002/2013JD020535,  
828 2014.

829 Bowen, G. J., Cai, Z., Fiorella, R. P. and Putman, A. L.: Isotopes in the Water Cycle: Regional-  
830 to Global-Scale Patterns and Applications, *Annu. Rev. Earth Planet. Sci.*, 47(1), 453–479,  
831 doi:10.1146/annurev-earth-053018-060220, 2019.

832 Cai, Y., Cheng, H., An, Z., Edwards, R. L., Wang, X., Tan, L. and Wang, J.: Large variations of  
833 oxygen isotopes in precipitation over south-central Tibet during Marine Isotope Stage 5,  
834 *Geology*, 38(3), 243–246, doi:10.1130/G30306.1, 2010.

835 Chakraborty, S., Sinha, N., Chattopadhyay, R., Sengupta, S., Mohan, P. M. and Datye, A.:  
836 Atmospheric controls on the precipitation isotopes over the Andaman Islands, Bay of Bengal,  
837 *Sci. Rep.*, 6, 19555 [online] Available from: <https://doi.org/10.1038/srep19555>, 2016.

838 Christner, E., Aemisegger, F., Pfahl, S., Werner, M., Cauquoin, A., Schneider, M., Hase, F.,  
839 Barthlott, S. and Schädler, G.: The Climatological Impacts of Continental Surface Evaporation,  
840 Rainout, and Subcloud Processes on  $\delta$ D of Water Vapor and Precipitation in Europe, *J.*  
841 *Geophys. Res. Atmos.*, 123(8), 4390–4409, doi:10.1002/2017JD027260, 2018.

842 Clark, I. D. and Fritz, P.: *Environmental Isotopes in Hydrogeology*, Lewis, Boca Raton, Florida.,  
843 1997.

844 Craig, H.: Isotopic Variations in Meteoric Waters, *Science* (80-. ), 133(3465), 1702–1703, 1961.  
845 Dansgaard, W.: Stable isotopes in precipitation, *Tellus*, 16(4), 436–468,  
846 doi:10.3402/tellusa.v16i4.8993, 1964.

847 Deshpande, R. D., Maurya, A. S., Kumar, B., Sarkar, A. and Gupta, S. K.: Rain-vapor  
848 interaction and vapor source identification using stable isotopes from semiarid western India, *J.*  
849 *Geophys. Res. Atmos.*, 115(23), 1–11, doi:10.1029/2010JD014458, 2010.

850 Deshpande, R. D., Maurya, A. S., Kumar, B., Sarkar, A. and Gupta, S. K.: Kinetic fractionation  
851 of water isotopes during liquid condensation under super-saturated condition, *Geochim.*  
852 *Cosmochim. Acta*, 100, 60–72, doi:https://doi.org/10.1016/j.gca.2012.10.009, 2013.

853 Fiorella, R. P., Bares, R., Lin, J. C., Ehleringer, J. R. and Bowen, G. J.: Detection and variability  
854 of combustion-derived vapor in an urban basin, *Atmos. Chem. Phys.*, 18(12), 8529–8547,  
855 doi:10.5194/acp-18-8529-2018, 2018.

856 Fisher, D. A.: Remarks on the deuterium excess in precipitation in cold regions, *Tellus B*, 43(5),  
857 401–407, doi:https://doi.org/10.1034/j.1600-0889.1991.t01-4-00006.x, 1991.

858 Froehlich, K., Kralik, M., Papesch, W., Rank, D., Scheifinger, H. and Stichler, W.: Deuterium  
859 excess in precipitation of Alpine regions – moisture recycling, *Isotopes Environ. Health Stud.*,  
860 44(1), 61–70, doi:10.1080/10256010801887208, 2008.

861 Gat, J. R.: OXYGEN AND HYDROGEN ISOTOPES IN THE HYDROLOGIC CYCLE, *Annu.*  
862 *Rev. Earth Planet. Sci.*, 24(1), 225–262, doi:10.1146/annurev.earth.24.1.225, 1996.

863 Gorski, G., Strong, C., Good, S. P., Bares, R., Ehleringer, J. R. and Bowen, G. J.: Vapor  
864 hydrogen and oxygen isotopes reflect water of combustion in the urban atmosphere, *Proc. Natl.*  
865 *Acad. Sci.*, 112(11), 3247–3252, doi:10.1073/pnas.1424728112, 2015.

866 Graf, P., Wernli, H., Pfahl, S. and Sodemann, H.: A new interpretative framework for below-  
867 cloud effects on stable water isotopes in vapour and rain, *Atmos. Chem. Phys.*, 19(2), 747–765,  
868 doi:10.5194/acp-19-747-2019, 2019.

869 Guan, H., Zhang, X., Skrzypek, G., Sun, Z. and Xu, X.: Deuterium excess variations of rainfall  
870 events in a coastal area of south Australia and its relationship with synoptic weather systems  
871 and atmospheric moisture sources, *J. Geophys. Res. Atmos.*, 118(2), 1123–1138,  
872 doi:10.1002/jgrd.50137, 2013.

873 Jacob, H. and Sonntag, C.: An 8-year record of the seasonal variation of 2 H and 18 O in  
874 atmospheric water vapour and precipitation at Heidelberg, Germany, *Tellus B Chem. Phys.*  
875 *Meteorol.*, 43(3), 291–300, doi:10.3402/tellusb.v43i3.15276, 1991.

876 Jeelani, G., Deshpande, R. D., Galkowski, M. and Rozanski, K.: Isotopic composition of daily  
877 precipitation along the southern foothills of the Himalayas: Impact of marine and continental  
878 sources of atmospheric moisture, *Atmos. Chem. Phys.*, 18(12), 8789–8805, doi:10.5194/acp-  
879 18-8789-2018, 2018.

880 Jouzel, J. and Merlivat, L.: Deuterium and oxygen 18 in precipitation: Modeling of the isotopic  
881 effects during snow formation, *J. Geophys. Res.*, 89(D7), 11749, doi:10.1029/jd089id07p11749,  
882 1984.

883 Jouzel, J., Delaygue, G., Landais, A., Masson-Delmotte, V., Risi, C. and Vimeux, F.: Water

884 isotopes as tools to document oceanic sources of precipitation, *Water Resour. Res.*, 49(11),  
885 7469–7486, doi:<https://doi.org/10.1002/2013WR013508>, 2013.

886 Li, L. and Garzione, C. N.: Spatial distribution and controlling factors of stable isotopes in  
887 meteoric waters on the Tibetan Plateau : Implications for paleoelevation reconstruction, *Earth*  
888 *Planet. Sci. Lett.*, 460, 302–314, doi:[10.1016/j.epsl.2016.11.046](https://doi.org/10.1016/j.epsl.2016.11.046), 2017.

889 Li, Z., Qi, F., Wang, Q. J., Kong, Y., Cheng, A., Song, Y., Li, Y., Li, J. and Guo, X.: Contributions  
890 of local terrestrial evaporation and transpiration to precipitation using  $\delta^{18}\text{O}$  and D-excess as  
891 a proxy in Shiyang inland river basin in China, *Glob. Planet. Chang.*, 146, 140–151, 2016.

892 Liu, W., Feng, X., Liu, Y., Zhang, Q. and An, Z.:  $\delta^{18}\text{O}$  values of tree rings as a proxy of monsoon  
893 precipitation in arid Northwest China, *Chem. Geol.*, 206(1), 73–80,  
894 doi:<https://doi.org/10.1016/j.chemgeo.2004.01.010>, 2004.

895 Liu, W., Liu, H., Wang, Z., An, Z. and Cao, Y.: Hydrogen isotopic compositions of long-chain  
896 leaf wax n-alkanes in Lake Qinghai sediments record palaeohydrological variations during the  
897 past 12 ka, *Quat. Int.*, 449, 67–74, doi:<https://doi.org/10.1016/j.quaint.2017.05.024>, 2017a.

898 Liu, W., Wang, H., Leng, Q., Liu, H., Zhang, H. and Xing, M.: Hydrogen isotopic compositions  
899 along a precipitation gradient of Chinese Loess Plateau : Critical roles of precipitation /  
900 evaporation and vegetation change as controls for leaf wax  $\delta\text{D}$ , *Chem. Geol.*, 528(April),  
901 119278, doi:[10.1016/j.chemgeo.2019.119278](https://doi.org/10.1016/j.chemgeo.2019.119278), 2019.

902 Liu, Y., Liu, H., Song, H., Li, Q., Burr, G. S., Wang, L. and Hu, S.: A monsoon-related 174-year  
903 relative humidity record from tree-ring  $\delta^{18}\text{O}$  in the Yaoshan region, eastern central China, *Sci.*  
904 *Total Environ.*, 593–594, 523–534, doi:<https://doi.org/10.1016/j.scitotenv.2017.03.198>, 2017b.

905 Merlivat, L. and Jouzel, J.: Global climatic interpretation of the deuterium-oxygen 18 relationship  
906 for precipitation, *J. Geophys. Res. Ocean.*, 84(C8), 5029–5033,  
907 doi:<https://doi.org/10.1029/JC084iC08p05029>, 1979.

908 Peng, T. R., Liu, K. K., Wang, C. H. and Chuang, K. H.: A water isotope approach to assessing  
909 moisture recycling in the island-based precipitation of Taiwan: A case study in the western  
910 Pacific, *Water Resour. Res.*, 47(8), 1–11, doi:[10.1029/2010WR009890](https://doi.org/10.1029/2010WR009890), 2011.

911 Putman, A. L., Fiorella, R. P., Bowen, G. J. and Cai, Z.: A Global Perspective on Local Meteoric  
912 Water Lines-SM, *Water Resour. Res.*, 1–6, doi:[10.1351/pac198961081483.Jaffey](https://doi.org/10.1351/pac198961081483.Jaffey), 2019a.

913 Putman, A. L., Fiorella, R. P., Bowen, G. J. and Cai, Z.: A Global Perspective on Local Meteoric  
914 Water Lines: Meta-analytic Insight into Fundamental Controls and Practical Constraints, *Water*  
915 *Resour. Res.*, 2019WR025181, doi:[10.1029/2019WR025181](https://doi.org/10.1029/2019WR025181), 2019b.

916 Rangarajan, R., Laskar, A. H., Bhattacharya, S. K., Shen, C. C. and Liang, M. C.: An insight  
917 into the western Pacific wintertime moisture sources using dual water vapor isotopes, *J. Hydrol.*,  
918 547, 111–123, doi:[10.1016/j.jhydrol.2017.01.047](https://doi.org/10.1016/j.jhydrol.2017.01.047), 2017.

919 Salamalikis, V., Argiriou, A. A. and Dotsika, E.: Isotopic modeling of the sub-cloud evaporation  
920 effect in precipitation, *Sci. Total Environ.*, 544, 1059–1072, doi:[10.1016/j.scitotenv.2015.11.072](https://doi.org/10.1016/j.scitotenv.2015.11.072),  
921 2016.

922 Salmon, O. E., Welp, L. R., Baldwin, M. E., Hajny, K. D., Stirm, B. H. and Shepson, P. B.:  
923 Vertical profile observations of water vapor deuterium excess in the lower troposphere, *Atmos.*

924 Chem. Phys., 19(17), 11525–11543, doi:10.5194/acp-19-11525-2019, 2019.

925 Steen-Larsen, H. C., Johnsen, S. J., Masson-Delmotte, V., Stenni, B., Risi, C., Sodemann, H.,  
 926 Balslev-Clausen, D., Blunier, T., Dahl-Jensen, D., Ellehøj, M. D., Falourd, S., Grindsted, A.,  
 927 Gkinis, V., Jouzel, J., Popp, T., Sheldon, S., Simonsen, S. B., Sjolte, J., Steffensen, J. P.,  
 928 Sperlich, P., Sveinbjörnsdóttir, A. E., Vinther, B. M. and White, J. W. C.: Continuous monitoring  
 929 of summer surface water vapor isotopic composition above the Greenland Ice Sheet, Atmos.  
 930 Chem. Phys., 13(9), 4815–4828, doi:10.5194/acp-13-4815-2013, 2013.

931 Stewart, M. K.: Stable isotope fractionation due to evaporation and isotopic exchange of falling  
 932 waterdrops: Applications to atmospheric processes and evaporation of lakes, J. Geophys. Res.,  
 933 80(9), 1133–1146, doi:10.1029/JC080i009p01133, 1975.

934 Sun, C., Chen, W., Chen, Y. and Cai, Z.: Stable isotopes of atmospheric precipitation and its  
 935 environmental drivers in the Eastern Chinese Loess Plateau, China, J. Hydrol., 581(November  
 936 2019), 124404, doi:10.1016/j.jhydrol.2019.124404, 2020.

937 Tan, L., An, Z., Huh, C.-A., Cai, Y., Shen, C.-C., Shiau, L.-J., Yan, L., Cheng, H. and Edwards,  
 938 R. L.: Cyclic precipitation variation on the western Loess Plateau of China during the past four  
 939 centuries, Sci. Rep., 4(1), 6381, doi:10.1038/srep06381, 2014.

940 Thompson, L. G., Yao, T., Mosley-Thompson, E., Davis, M. E., Henderson, K. A. and Lin, P.-  
 941 N.: A High-Resolution Millennial Record of the South Asian Monsoon from Himalayan Ice Cores,  
 942 Science (80-. ), 289(5486), 1916 LP – 1919, doi:10.1126/science.289.5486.1916, 2000.

943 Tian, C., Wang, L., Kaseke, K. F. and Bird, B. W.: Stable isotope compositions ( $\delta^2\text{H}$ ,  $\delta^{18}\text{O}$   
 944 and  $\delta^{17}\text{O}$ ) of rainfall and snowfall in the central United States, Sci. Rep., (October 2017), 1–  
 945 15, doi:10.1038/s41598-018-25102-7, 2018.

946 Wan, H., Liu, W. and Xing, M.: Isotopic composition of atmospheric precipitation and its tracing  
 947 significance in the Laohequ Basin, Loess plateau, China, Sci. Total Environ., 640–641(May),  
 948 989–996, doi:10.1016/j.scitotenv.2018.05.338, 2018.

949 Wang, S., Zhang, M., Che, Y., Chen, F. and Fang, Q.: Contribution of recycled moisture to  
 950 precipitation in oases of arid central Asia: A stable isotope approach, Water Resour. Res., 52(4),  
 951 3246–3257, doi:10.1002/2015WR018135, 2016a.

952 Wang, S., Zhang, M., Che, Y., Zhu, X. and Liu, X.: Influence of Below-Cloud Evaporation on  
 953 Deuterium Excess in Precipitation of Arid Central Asia and Its Meteorological Controls, J.  
 954 Hydrometeorol., 17(7), 1973–1984, doi:10.1175/JHM-D-15-0203.1, 2016b.

955 Wang, S., Zhang, M., Hughes, C. E., Crawford, J., Wang, G., Chen, F., Du, M., Qiu, X. and  
 956 Zhou, S.: Meteoric water lines in arid Central Asia using event-based and monthly data, J.  
 957 Hydrol., 562(May), 435–445, doi:10.1016/j.jhydrol.2018.05.034, 2018a.

958 Wang, Z., An, Z., Liu, Z., Qiang, X., Zhang, F. and Liu, W.: Hydroclimatic variability in loess  
 959  $\delta\text{D}_{\text{wax}}$  records from the central Chinese Loess Plateau over the past 250 ka, J. Asian Earth  
 960 Sci., 155, 49–57, doi:https://doi.org/10.1016/j.jseaes.2017.11.008, 2018b.

961 Welp, L. R., Lee, X., Kim, K., Griffis, T. J., Billmark, K. A. and Baker, J. M.:  $\delta^{18}\text{O}$  of water  
 962 vapour, evapotranspiration and the sites of leaf water evaporation in a soybean canopy, Plant,  
 963 Cell Environ., 31(9), 1214–1228, doi:10.1111/j.1365-3040.2008.01826.x, 2008.



964 Wen, X. F., Zhang, S. C., Sun, X. M., Yu, G. R. and Lee, X.: Water vapor and precipitation  
965 isotope ratios in Beijing, China, *J. Geophys. Res. Atmos.*, 115(1), 1–10,  
966 doi:10.1029/2009JD012408, 2010.

967 Wu, H., Fu, C., Zhang, C., Zhang, J., Wei, Z. and Zhang, X.: Temporal Variations of Stable  
968 Isotopes in Precipitation from Yungui Plateau: Insights from Moisture Source and Rainout Effect,  
969 *J. Hydrometeorol.*, 23(1), 39–51, doi:10.1175/JHM-D-21-0098.1, 2022.

970 Wu, J., Li, P. and Qian, H.: Variation characteristics of meteorological elements and prediction  
971 model of available precipitation in Xi'an city, *South-to-North water Transf. water Sci. Technol.*,  
972 11(001), 50–54, 2013.

973 Xing, M., Liu, W., Li, X., Zhou, W., Wang, Q., Tian, J., Li, X., Tie, X., Li, G., Cao, J., Bao, H. and  
974 An, Z.: Vapor isotopic evidence for the worsening of winter air quality by anthropogenic  
975 combustion-derived water, *Proc. Natl. Acad. Sci.*, 117(52), 33005–33010,  
976 doi:10.1073/pnas.1922840117, 2020.

977 Yao, T., Thompson, L. G., Mosley-Thompson, E., Zhihong, Y., Xingping, Z. and Lin, P.-N.:  
978 Climatological significance of  $\delta^{18}\text{O}$  in north Tibetan ice cores, *J. Geophys. Res. Atmos.*,  
979 101(D23), 29531–29537, doi:10.1029/96JD02683, 1996.

980 Yao, T., Masson-Delmotte, V., Gao, J., Yu, W., Yang, X., Risi, C., Sturm, C., Werner, M., Zhao,  
981 H., He, Y., Ren, W., Tian, L., Shi, C. and Hou, S.: A review of climatic controls on  $\delta^{18}\text{O}$  in  
982 precipitation over the Tibetan Plateau: Observations and simulations, *Rev. Geophys.*, 51(4),  
983 525–548, doi:10.1002/rog.20023, 2013.

984 Zhao, L., Liu, X., Wang, N., Kong, Y., Song, Y., He, Z., Liu, Q. and Wang, L.: Contribution of  
985 recycled moisture to local precipitation in the inland Heihe River Basin, *Agric. For. Meteorol.*,  
986 271(July 2018), 316–335, doi:10.1016/j.agrformet.2019.03.014, 2019.

987 Zhu, G. F., Li, J. F., Shi, P. J., He, Y. Q., Cai, A., Tong, H. L., Liu, Y. F. and Yang, L.:  
988 Relationship between sub-cloud secondary evaporation and stable isotope in precipitation in  
989 different regions of China, *Environ. Earth Sci.*, 75(10), 876, 2016.

990